An in vivo CRISPR screen unveils top target genes to efficiently improve CAR-T cell persistence in a solid tumour model of lung adenocarcinoma

Mattia Fumagalli[1,2,3*], Dongjie An[1,2], Luca Simula[1,2], Camille Combe[1,2], Lisa Aziez[1], Yannick Simoni[1], Marie-Clotilde Alves-Guerra[1], Andrea Valentini[4], Maude Marchais[1], Anaïs Vermare[1,2], Nadège Bercovici[1,2], Emmanuel Donnadieu[1,2] and Frédéric Pendino[1,2*]

[1] Université Paris Cité, Institut Cochin, INSERM, CNRS, F-75014 Paris, France
[2] Equipe Labélisée Ligue Nationale Contre le Cancer
[3] Thèse financée par la Ligue Nationale Contre le Cancer
[4] Technical University of Denmark, 2800 Kgs. Lyngby, Denmark
* Correspondence: frederic.pendino@inserm.fr and mattia.fumagalli@inserm.fr

ABSTRACT

CAR-T cell therapies are revolutionizing the treatment of refractory and relapsed haematological malignancies, but many patients do not exhibit long-term responses, and these therapies are less effective against solid tumours. Poor persistence of CAR-T cells in patients is associated with therapeutic failure, highlighting the need to identify genes that promote *in vivo* expansion. Here, we developed an accessible *in vivo* competitive screening method to identify genes whose inactivation provides a selective advantage to CAR-T cells. Inactivation of 50 genes in a heterogeneous population of T cells expressing an EGFR-targeting CAR revealed that disruption of *REGNASE-1, SOCS1, PTPN2*, and *P16INK4A* conferred a selective advantage to CAR-T cells in human lung tumour-bearing mice. Coherently, inactivation of these genes resulted in improved tumour eradication by CAR-T cells. Interestingly disruption of other genes, described to improve CAR-T cell function against other tumours, had a negative impact in this orthotropic lung tumour model. Further evaluation of late effects, within a subcutaneous model, highlighted *SOCS1* gene inactivation as the most promising strategy for *in vivo* CAR-T cell persistence. These results support the importance of evaluating CAR-T cell editing strategies in specific tumours models and the screening method proposed provides a versatile pre-clinical tool for assessing persistence and function in context-specific settings.

INTRODUCTION

In the field of Onco-Immunology, Chimeric Antigen Receptor (CAR)-T cells are imposing themselves as an efficient way to treat highly refractory leukaemia and lymphomas, obtaining complete remission in around 50% of the patients. Yet, an important fraction of patients still does not respond to these approaches, and despite recent encouraging successes, CAR-T therapy efficacy is limited in most solid tumours.[1] Follow up studies on first CAR-T clinical trials in lymphomas and leukaemia have shown that a poor expansion and persistence of CAR-T cells in the patient are the first predictive factors for a poor prognostic outcome.[2] Coherently, the data from the first clinical trials of CAR-T cells against solid tumours report thousands of times less CAR-T cells in the blood and the rare tumour biopsies of the patients compared to successful anti-CD19 CAR-T therapies and a much shorter persistence.[3, 4] On the contrary, in different occasional successful clinical trials of CAR-T against solid tumours [5] and in recent larger studies on anti-GD2 CAR-T cells or anti-IL13Ralpha2 in glioblastoma, cells numbers in the blood were comparable to those of successful anti-CD19 CAR-T therapies, and responding patients coherently showed better CAR-T expansion and persistence.[6, 7] Such observations in solid tumours suggest that while other complex factors participate in CAR-T cells efficacy in different contexts, including for example their capacity to infiltrate within the tumour or to resist to immunosuppression, good proliferation and persistence are ultimately essential. [4, 8]

Amelioration of CAR-T cells therapy is currently being pursued through several strategies and gene editing approaches are among the most promising.[8-10] Several research groups have shown that the ablation of some genes, encoding transcription factors (IKFZ3, BATF...)[11, 12], epigenetic modulators (DNMT3A, TET2...),[13, 14] signalling regulators (*SOCS1*, DGK-alpha/zeta...)[15, 16] or immunomodulatory receptors (PD1, TIM3...)[17, 18] could result in improvement of T or CAR-T cells efficacy with enhanced expansion or persistence in some *in vitro* or *in vivo* therapy models. Such results are really promising, but they have been obtained in different conditions, in terms, of CAR structure, target antigen, manufacture protocol or tumour model. Since all these elements have been proven too deeply influence CAR-T cells efficacy, it is impossible to compare the effects of these different gene candidates from these different studies.[19-23]

Whole genome screenings on T cells or CAR-T cells theoretically could allow to identify which gene KO provide the clearest advantages. Such approaches have been successfully applied for discovery purposes, allowing the identification of new potential candidates target genes for T or CAR-T cells amelioration. [24-31] Nonetheless, results are not, or only partially, consistent among these different screenings, suggesting that specific characteristics of different models can influence results, arguing in favour of the need for context-specific analyses, in as relevant as possible preclinical models. Unfortunately, technical limitations, such as poor infiltration in tumour tissues or reduced in situ proliferation, especially challenging in *in vivo* solid cancer models,[32] make so that whole genome approaches would be hardly applicable for specific studies on given CAR-T cells in given contexts. Notably large gRNA libraries used in such screenings (up to around a hundred thousand sgRNAs) generally force tailored experimental settings, expensive and time-consuming sequencing pipelines. [27, 29]

We propose a new strategy to compare genetic ameliorations in CAR-T cells, by re-purposing the CRISPR-KO screening approach for comparison on a selected group of 50 top potential target genes. Such an approach allows for reductions in costs, time and complexity of screening experiments, making it a versatile pre-clinical tool, for improving specific CAR-T therapies in specific contexts. We applied such strategy for the improvement of CAR-T cells in models of non-small cells lung adenocarcinoma, a promising yet challenging solid tumour target for CAR-T therapy development.[33, 34]

RESULTS

Set up of a CRISPR-Cas9 system to edit 50 top target genes in a pool of CAR-T cells and a method to quantify subpopulations.

By an extensive search in the literature performed in march 2023, we defined a list of 50 genes with known or putative functions in T or CAR T cells and whose inactivation could increase their proliferation, persistence and long-term efficiency.[11-18, 24-27, 29-31, 35-68] (Tab. 1) Then, we set up a method to integrate gene editing in the CAR-T cells production pipeline. Briefly T cells are first transduced with a pool of lentiviral vectors expressing a total of 236 gRNAs, then transduced with the CAR vector, and finally nucleofected with the Cas9 protein. This strategy allows us to produce a pool of CAR-T cells each carrying an inactivating mutation in one of the selected genes (Fig. 1 A). First, we validated this editing system in a pilot experiment, targeting *EGFP* (enhanced Green Fluorescent Protein) and testing the editing by cytofluorimetric analysis of protein expression (Fig 1 B). Then, we assessed the editing of a gene encoding an epigenetic factor, *RINF*, expressed at low levels in T-cells, for which we confirmed effective editing at a genomic level by TIDE (Tracking of Indels by Decomposition) assay (Fig 1 C). Then we produced the lentiviral vectors library, and we set up quantification of CAR-T Knockout (KO) subpopulations by targeted Next Generation Sequencing (NGS), of sgRNA coding regions in the lentiviral vectors and bioinformatic analysis through MAGeCK (Model-based Analysis of Genome-wide CRISPR-Cas9 Knockout) algorithm.[6] We could verify the efficiency of our library by measuring the effect of sgRNA targeting genes of the T cells activation signalling cascade, previously defined as essential in whole genome CRISPR-KO studies.[24, 26] CAR-T cells inactivated for these negative control genes, *ZAP70, RHOH, LCP2* and *VAV1*, are all significantly negatively selected upon anti-CD3/CD28 driven *in vitro* expansion of CAR-T cells (Fig 1 D,E). Interestingly among the candidate genes selected in this screening, some are well known negative regulators of the TCR (T cell receptor) pathway. Among these genes, *CBL-B, CD5, DGK-Z, DGK-A, RASA2* are significantly, though slightly, positively selected during this short-term *in vitro* expansion essay (Fig 1 E). These results validate our editing system, the lentiviral bank as well as the targeted NGS sequencing strategy and bioinformatic pipeline employed for the analysis.

Set up and validation of a relevant in vivo orthotopic tumour model of CAR-T therapy.

We produced second generation CAR-T cells targeting the antigen EGFR and having a 41BB co-stimulatory domain. We confirmed that cells transduced with this CAR construct efficiently and specifically target EGFR expressing tumour cells. (Supplementary Fig. 1 A, B) The EGFR antigen is expressed by different solid tumours, including the A549 lung cancer cell line. We used this cell line to establish an orthotopic model of lung tumour in NSG (NOD severe combined immune deficiency gamma mouse) mice with luciferase-expressing A549 cells that develop tumour-islets in mice lungs. (Fig. 2 A, B, C). We could verify that our CAR-T cells can effectively infiltrate and accumulate in such tumour islets to higher proportion than in surrounding lung regions, as measured by immunofluorescence analysis. (Fig. 2 B, Supplementary fig. 1 C) Then we validated that CAR-T cells could specifically control and eradicate tumours in vivo, as defined by bioluminescence analysis. (Fig. 2 D). We could detect CAR-T cells in lung tumours at the experiment's endpoint and isolate them so to perform cytofluorimetric analysis and functional assays. Even in the favourable conditions of such pilot experiment, we could detect on these CAR-T cells a clear upregulation of differentiation markers, activation and exhaustion markers as compared to the same CAR-T before injection (Fig. 2 E, Supplementary fig. 1 D). Coherently such cells show reduced cytotoxicity and proliferation indicating that long term tumour exposure in this model can induce a dysfunctional state in CAR-T cells (Fig. 2 F). Interestingly, by gathering data from different experiments, we could observe that in such a model, CAR-T cells number in mice lung at the endpoint of the experiment and the tumour charge as defined by bioluminescence imaging, show a strong inverse

correlation (Fig. 2 G). Such relation appears to be stronger than an inverse linear correlation, and could instead be described by a power law, as we could demonstrate by statistical data fitting (Fig. 2 G). Such observation allows to confirm a very strong relation among persistence/proliferation of CAR-T cells and tumour prognosis in this model, with small changes in CAR-T abundance having a great impact on tumour prognosis according to the power law. Overall, these analyses, support the pertinence of this orthotopic lung tumour model for the proposed study.

The In vivo CRISPR-KO screening assay allows to define, among 50 top candidate genes, those whose KO gives the clearest selective advantage to CAR-T cells

We so proceeded to carry out our *in vivo* screening assay. Briefly we injected tumour-bearing mice with CAR-T cells edited to carry mutations in one of the 50 candidate genes, the 4 negative control genes, or no mutations for those transduced with control sgRNA expressing plasmids (Fig. 3 A). We defined conditions to obtain tumour control without eradication and to increase the power of the test, we produced CAR-T cells starting from the blood of three different donors. For CAR-T cells from each donor, we could obtain sub-optimal therapy conditions, allowing tumour control but not eradication (Fig. 3 B). At the endpoint of the experiments, we could detect meaningful proportions of CAR-T in the lungs,(Fig. 3 C) which allowed us to proceed to identify CAR-T cells subpopulations by NGS (Next Generation Sequencing). Briefly, from DNA extracts of the tumour bearing mice lungs, we amplified the sgRNA expressing region of lentiviral vectors, inside CAR-T cells. PCR amplicons underwent NGS sequencing and raw data were analysed with MAGeCK, a bioinformatic tool for gene ranking according to sgRNAs frequency.

In tumour samples, most of sgRNAs could be detected, even in samples with very low car-t cells numbers, proving the good sensibility of our approach (Supplementary fig. 2 A). By MAGeCK analysis, we could define a positively selected sgRNAs, and therefore gene targets, significantly enriched in different tumour samples of mice receiving CAR-T cells from given blood donors. (Fig. 3 D) Most importantly, sgRNA for the KO of some genes, notably *REGNASE-1, SOCS1, PTPN2 and P16INK4A*, led to a robust selective advantage of CAR-T cells consistently among the three different donors CAR-T cells. (Fig. 3 E) Surprisingly, while sgRNAs targeting essential T-cell activation genes led to a negative selection as expected, some putative target genes for CAR-T cells amelioration, notably *MED12, PRDM1*, and *BATF* scored as bad or even worse than these negative controls, coherently through different donors. These genes, while increasing CAR-T cells proliferation/persistence in the experimental conditions of the respective studies,[11, 26, 52] appear rather to impair such capacities in these specific conditions. (Fig. 3 E).

Throughout the setting up of such screening, we performed different assays with CAR-T cells from the same donor, but adjusting conditions to create settings more or less favourable to CAR-T cells. Interestingly, we could observe that in an experiment where CAR-T cells obtain rapid eradication of tumours, and therefore undergo minimal selective pressure, no meaningful effect could be observed in term of gene-ko subpopulations selection. (Fig. 3 F left, Supplementary fig. 2 B) However, in more challenging conditions we could observe more pronounced effects on gene-ko subpopulations enrichment, (Fig. 3 F middle and right, Supplementary fig. 2 B) proving that these outcomes are strictly dependent on selective pressure and specific to CAR-T cells exposure to tumour.

Overall, these screening results demonstrate the feasibility of our approach and strongly advocate for the convenience of assessing the effects of gene editing strategies on specific CAR-T cells and contexts, as close as possible to the actual therapy.

174 ***Individual KO of screening top hits REGNASE-1 and PTPN2 confers improved tumour capacities to***
175 ***CAR-T cells***

176 We then sought to confirm that the selective advantage we observed for the top hits of our screening,
177 could actually translate into an increased tumour control capacity *in vivo*. We so designed lentiviral
178 vectors expressing gRNAs targeting *PTPN2* and *REGNASE-1*, two out of the 4 most reproductible gene
179 hits across different donor and stress conditions. Despite a relatively suboptimal gene editing
180 efficiency, (Supplementary fig. 3 A), both *REGNASE-1* KO and *PTPN2* KO CAR-T cells showed a clearly
181 improved anti-tumour capacity. Comparing to mice injected with CTRL CAR-T cells, we could obtain,
182 for both gene-ko strategies, a notably better control of tumour growth, leading to a significantly better
183 survival. (Fig. 4 A, B) Confirming our assumption that an increased persistence of CAR-T cells in a model
184 of stress conditions, would correlate with increased antitumour efficacy.

185 Mice were than sacrificed at 28 days to allow comparison with the control condition. First, we could
186 confirm a strongly reduced tumour charge in mice lungs from both *PTPN2* KO and *REGNASE-1* KO mice
187 as compared to mice treated with ctrl CAR-T cells that survived to the end of the experiment. (Fig. 4 C)
188 We could detect significantly higher numbers of *REGNASE-1* KO CAR-T cells, both in the tumour site
189 and circulating lymphoid organ, as assessed in the spleen. On the other hand, *PTPN2* KO seemed to
190 have no significant impact on CAR-T cell proliferation. (Fig. 4 D) While absence of data from deceased
191 CTRL mice may be a source of bias, such data suggests that different mechanisms could explain the
192 improved tumour control conferred by the KO of the two genes. Targeting *REGNASE-1* appears to have
193 a marked effect on CAR-T cells expansion *in vivo* in this model. Conversely *PTPN2* inactivation may
194 have a different impact, providing a selective advantage to CAR-T cells in stress conditions, without
195 leading to excessive CAR-T cells accumulation in a more favourable context. Collectively, both
196 mechanisms ultimately resulting in improved persistence upon tumour engagement and increased
197 tumour control.

198 ***REGNASE-1 KO CAR-T cells retain sensibility to safety switch systems iCas9 suicide gene, allowing for***
199 ***a safer implementation of proliferation increasing gene editing strategies***

200 While the great number of *REGNASE-1* KO CAR-T cells detectable both in the tumour site, the lungs,
201 and in circulating lymphoid organs, as assed in the spleen, (Fig. 4 D) could ensure an effective response
202 against the tumour, it also raises the question of potential toxicities. Indeed, in previous papers
203 published on this genetic modification in CAR-T cells, when combined to *ROQUIN* KO, over-
204 proliferation of CAR-T cells was observed and associated with toxicity.[69] To address this potential
205 issue, we sought to test feasibility of implementation of the safety switch system iCas9,[70] that has
206 been successfully applied in clinics, in gene edited CAR-T cells.[6] We produced CAR-T cells equipped
207 with a vector expressing human caspase-9 protein fused with a FK506-binding protein 12 (with F36V
208 mutation), to allow dimerization upon administration of a small dimerizing agent AP02187, and we
209 combined such modification with *REGNASE-1* KO by Ribonucleoprotein complex nucleofection. Of
210 note, to maximize editing efficiency, we used a double gRNA approach, with recently described highly
211 effective *REGNASE-1* targeting sequences. (Supplementary fig. 3 B) We could assess that upon
212 dimerization induction, a rapid and efficient mortality is obtained, even in active, proliferating CAR-T
213 cells, reducing living cells numbers to below 10% within 24 hours, with no difference among modified
214 and non-modified CAR-T cells. (Fig. 4 E) Such results indicate that the iCas9 system could likely assure a
215 rapid and efficient control of classical toxicities associated with potent CAR-T cells response, also for
216 *REGNASE-1* KO modified CAR-T cells.

217

Phenotypic characterisation of REGNASE-1 KO and PTPN2 KO CAR-T cells upon in Vivo exposure to tumour.

We then sought to better characterise *REGNASE-1* KO and *PTPN2* KO after exposure to tumour, looking for insights on their improved anti-tumour capacity. We so proceeded to CytOF (Cytometry by time of flight) characterisation of CAR-T cells extracted from the tumour site, mice lungs. To analyse data, we proceeded to UMAP(Uniform Manifold Approximation and Projection) analysis, to summarize information from more than 30 markers. First, we could assess that despite a certain variability among replicates, CAR-T cells from each group show a similar clustering. (Supplementary fig. 4 A) We so focused cluster analysis on three exemplary samples and then confirmed the presence of clusters and variations determining them, on all replicates. (Fig. 5 A, Supplementary fig. 4 A) Overall, UMAP analysis clearly identifies 4 major clusters, one large CD4 cluster, one large CD8 cluster, a group of cells expressing both CD4 and CD8, referred to as double positive, and a very small cluster of double negative cells, which nonetheless express CD3. Regarding the different conditions, the major difference observed is an increased percentage of CD4 for *PTPN2* KO CAR-T cells and more clearly for *REGNASE-1* KO CAR-T cells. (Fig. 5 A, Supplementary fig. 4 A)

In addition, CTRL CAR-T and *REGNASE-1* KO CAR-T cells more clearly differ, while *PTPN2* KO cells mostly resemble to CTRL cells. (Fig. 5 A, Supplementary fig. 4 A) The difference in *REGNASE-1* KO CAR-T cells consists in the formation of a large and well distinguished cluster within the CD4 group. This cluster is mostly characterised by the simultaneous expression of activation markers, specifically HLA-DR, ICOS, CD28 and immunomodulatory markers such as CTLA4, PD1 which are upregulated in *REGNASE-1* KO CAR-T cells. (Fig. 5 A, B Supplementary fig. 4B) At the same time, we could detect a clear expression of cytotoxic molecules on cells within this compartment, with some of these molecules, as granzyme A, expressed more broadly and at higher levels than in other CD4 cells. (Fig. 5 D). These highly active, cytotoxic CD4+ cells constitute a significantly larger portion of the total cell population in *REGNASE-1* KO CAR-T cells, suggesting that this subset may have played a fundamental role in the improved tumour control observed in mice receiving these CAR-T cells.

Within the CD8 cluster we could observe a similar change for *REGNASE-1* KO cells, with the emergence of a similar cluster, although less clearly defined. (Fig. 5 C) This subpopulation of cells is characterised by the same markers as their CD4 counterpart, including activation markers such a as HLA-DR, ICOS, CD28 and immunomodulatory markers like CTLA4, PD1, and appear to retain full cytotoxicity capacity. (Fig. 5 C, D) While representing a less important proportion of CD8 cells than the CD4 sub-cluster, this subpopulation can be clearly observed in all *REGNASE-1* KO and is significantly enriched when compared to CTRL CAR-T cells (Fig. 5 C, D, Supplementary fig. 4 C). CD8 T cells represent a smaller proportion of whole cell population in *REGNASE-1* KO CAR-T cells compared to CTRL cells. Nonetheless, despite the large overall increase in cell numbers observed in this condition, it appears that while *REGNASE-1* KO was more pronounced in CD4+ cells, it also has a notable effect on CD8+ cells.

Overall, KO of *REGNASE-1* appears to allow CAR-T cells to achieve and retain a stronger activation upon tumour encounter, which could explain the large increase in CAR-T cells numbers, while maintaining anti-tumour capacities, allowing for better tumour control and ultimately tumour clearance.

260 ***KO of MED12, the lowest-scoring gene in our screening, increase in vitro proliferation and***
261 ***differentiation but reduces in vivo persistence and long-term tumour control capacity***

262 As previously discussed, our *in vivo* screening gave unexpected results, showing that KO of at least 3
263 of the promising target genes we selected, was as deleterious as KO of the TCR signalling genes used
264 as negative control. The lowest scoring was *MED12*, therefore we sought to confirm that the ablation
265 of this gene could impair CAR-T cell tumour control in our model. We treated tumour bearing mice
266 with an "high" dose of CAR-T cells, either unmodified or KO for *MED12*. (Supplementary fig. 5 A) As
267 expected, at this dose the unmodified CAR-T cells could efficiently eradicate tumours within 21 days
268 post injection. At first, *MED12* KO CAR-T also could eradicate tumours in some mice and strongly
269 reduce tumour size in others. Nonetheless in *MED12* KO CAR-T treated mice tumours reappeared and
270 despite an initial control, the tumours that persisted ultimately grew back, leading to the death of most
271 of the mice. On the contrary only a single mouse of the ctrl CAR-T group showed a clear relapse, still
272 under control by the end of the experiment. (Fig. 6 A,B) According to these data, we could deduce that
273 *MED12* KO, in our specific conditions, does not clearly impair CAR-T functionality, but rather reduce
274 their long-term persistence. We therefore sought to further understand this effect and possibly align
275 our observations with previously published data on this genetic alteration in CAR-T cells. First, we
276 observed that CAR-T cells receiving *MED12*-targeting gRNAs in the screenings for all three donors
277 showed better expansion on average compared to other CAR-T cells during the production phase,
278 although there was minimal variation for the majority of genes. However, this ex vivo expansion is
279 more than compensated by the loss observed later during the in vivo phase, showing that this
280 modification could be beneficial under different conditions. (Fig. 6 C) Moreover, we could confirm this
281 in vitro proliferation during the production phase in an independent experiment with CAR-T cells from
282 the same three donors. (Supplementary fig. 5 B) We then proceeded to phenotypical characterisation of
283 these *MED12* KO CAR-T cells, and we could observe, as previously reported,[26] that these cells
284 exhibited a higher degree of differentiation compared to unmodified CAR-T cells by the end of the
285 production phase, especially characterised by a loss of stem cell memory T cells in both the CD4 and
286 CD8 compartments. (Fig. 6 D, Supplementary fig. 5 C) This increased differentiation could explain an
287 increased short-term proliferation but could as well have led to a reduced in vivo persistence, as
288 previously shown for more effector like CAR-T cells.

289 ***High selective pressure In vitro assay allows to reproduce in vivo screening results, despite less clear-***
290 ***cut effects***

291 Previous results overall confirmed the feasibility and the pertinence of our in vivo competitive
292 screening and confirmed the importance of performing such tests in a relevant context. Nonetheless,
293 we hypothesized that for studying some particular characteristics, in vitro surrogate tests could be
294 useful, as long as their results align with those obtained in the *in vivo* model. We therefore set up
295 conditions for a high selective pressure assay, restimulating CAR-T cells at a high frequency, every 5
296 days, in complete absence of cytokines in the culture medium, for 35 days. (Fig. 7 A) In such conditions
297 we could obtain an initial strong expansion of CAR-T cells, effectively eradicating tumour cells.
298 However, later on, we could observe stagnation followed by a clear reduction in CAR-T cells numbers.
299 (Fig. 7 B) We therefore considered the conditions of high selective pressure and proceeded to analyse
300 variations within gene-KO subpopulations. The results an obtained were similar to those observed in
301 vivo. We also observed *SOCS1, REGNASE-1, PTPN2* and *P16INK4A* KO remained the top-scoring genes,
302 despite their advantage over other genes was less pronounced, due to higher donor-to-donor
303 variability. The same applies to genes whose KO had a negative effect in the in vivo screenings,
304 however in this case their disadvantage appear even less consistent across donors. (Fig. 7 C,
305 Supplementary fig. 6 A)

306 ***Effects of signalling differences among TCR-like and CAR stimulation gene editing strategies efficacy***
307 ***in vitro***

308 Once tested the coherence of the developed in vitro assay as a surrogate for in vivo screening under
309 our conditions, we sought to apply it first to study the effects of signalling differences on gene editing
310 strategies efficacy. As many data derived from T-cells studies are often proposed for applications in
311 the CAR-T field, we wondered if the efficacy of gene editing strategies in improving CAR-T cell
312 expansion could be impacted by whether these cells are stimulated either through a TCR-like signal or
313 the CAR construct recognition of its antigen. In particular we focused on the effects on proliferation of
314 gene editing strategies impacting the TCR signalling pathway. To mimic TCR signalling, we used anti-
315 CD3/anti-CD28 loaded polymers, and we exposed CAR-T cells to irradiated tumour cells to stimulate
316 them through the CAR. Interestingly, we clearly observed that upon 14 days of proliferation, the KO
317 of essential TCR pathway genes had a significantly more marked negative effect in the TCR-like
318 stimulation condition compared to CAR stimulation. Even more clearly, the KO of TCR pathway
319 regulators had a significantly better effect in cells stimulated through the TCR, both in term of target
320 gene ranking as compared to other genes and actual fold change increase. (Fig. 7 D) Such results indicate
321 that while the CAR signalling is designed to mimic TCR signalling, differences between the two have
322 been described among them,[71, 72] and differences have a clear impact on the efficacy of gene
323 editing strategies.

324 ***CAR with either 41BB or CD28 co-stimulation domain show different persistence but similar response***
325 ***to gene editing strategies***

326 We then asked if the differences observed in the TCR-like stimulation and CAR stimulation screenings
327 could be explained by the different co-stimulation signal, since our CAR construct relies on a 41BB co-
328 stimulation. Moreover, co-stimulation with either CD28 or 41BB is to date one of the main differences
329 among different CAR-T products,[73, 74] it therefore constituted an interesting difference to
330 investigate. We redesigned our CAR construct to integrate a CD28 co-stimulation domain instead of
331 the 41BB domain. We tested these CAR- T cells using our in vitro re-stimulation assay and observed a
332 clear difference in the persistence of CD28 CAR-T cells compared to 41BB with CD28 CAR-T cells being
333 unable to persist until the endpoint of the experiment. (Fig. 7 D, Supplementary fig. 6 B) We so adapted
334 our re-stimulation test, reducing re-stimulation frequency to once every 7 to 10 days, to allow 35 days
335 long co-culture of both CD28 and 41BB CAR-T cells. (Supplementary fig. 6 C) In these conditions we could
336 observe an overall less marked selection of genes KO subpopulations, with only a partial reproduction
337 of previous results. Notably we again detected *SOCS1* and *PTPN2* as clear top-scoring genes, while the
338 KO of *REGNASE-1* and *P16INK4A* did not confer a clear advantage. (Fig. 7 E) Nonetheless, we clearly
339 observed no major differences between the two conditions, with *SOCS1* and *PTPN2* emerging as the
340 first and second-best scoring genes, respectively. (Fig. 7 E) These results confirm that as previously
341 described,[73, 75] also in our conditions, differences among 41BB and CD28 co-stimulation play a
342 major role on persistence of CAR-T cells. Nonetheless we did not observe an impact on gene editing
343 strategies on CAR-T cells proliferation and persistence.

344 ***A subcutaneous tumour model to study gene editing efficacy on longer term, within different tumour***
345 ***structure and for metastasis control***

346 We then translated our screening assay to different conditions in order to test its applicability in a
347 different *in vivo* model and gain insights into the effects of factors such as time and tumour structure
348 on the efficiency of gene editing strategies. Therefore, we developed a model relying again on the
349 A549 cell line, but developing a subcutaneous tumour, targeted by CAR-T cells with the same CAR
350 construct. First, we could verify a sufficient but less effective CAR-T cells tumour infiltration in this

351 model, leading to tumour control, without complete eradication. (Fig. 8 A,B) Coherently in this model,
352 we could observe a clear inverse correlation between tumour mass and CAR-T cells numbers, but such
353 relation appears less marked then in the lung tumour model. (Fig. 8 C) Similarly to the orthotopic model,
354 we characterised CAR-T cells extracted from mice tumours, and we could confirm upregulation of
355 differentiation and exhaustion markers on CAR-T cells and a clear impairment in functional assays.
356 (Supplementary fig. 7 A, B, C) Interestingly, we could observe that A549 cells subcutaneous tumours
357 develop lung metastases and CAR-T cells treatment can efficiently control and eliminate them in some
358 mice. (Fig. 8 D, E)

359 ***Screening in subcutaneous tumour model highlight clearer advantage for SOCS1 KO***

360 We repeated our screening in this subcutaneous model, mice were treated with modified CAR-T cells
361 and sacrificed 70 to 77 days after treatment. (Fig. 8 F) First we could detect sufficient CAR-T cells
362 infiltration in mice tumours from 2 out of 3 T donors, with a large variability in numbers of cells among
363 different samples, ranging from <0.1% to 30%.(Supplementary fig. 7 D) Nonetheless, we could perform
364 sequencing analysis on all these samples, and could not observe any clear relationship between
365 prevailing gene modifications and cells numbers. On the contrary, we observed positive or negative
366 selection for gene KO subpopulations. In this model we confirmed the top ranking of *SOCS1, PTPN2*
367 and *P16INK4*, while for *REGNASE-1* KO, we couldn't observe a consistent effect across the two donors.
368 (Fig. 8 G) Nonetheless, the most evident difference compared to the orthotopic lung tumour screening
369 is the significantly improved performance of *SOCS1* KO CAR-T cells compared to other modified
370 subpopulations. This suggests that such a genetic modification could provide a clearer advantage in
371 the long term, particularly against a more complex structured and limited infiltration. (Fig. 8 G)
372 Coherently, we again observed that the KO of genes *PRDM1* and *BATF* had a clearly negative impact,
373 whereas the effect of MED12 KO appeared less defined in this context. (Fig. 8 G)

374 ***Analysis of gene-ko subpopulation enriched in the lung as metastatic site***

375 We then analysed mice lungs as we observed the development of lung metastases in this model. We
376 could confirm the detection of CAR-T cells in the lungs, in roughly similar proportions to those observed
377 in the orthotopic tumour model. (Supplementary fig. 7 E) Additionally, in this context, we could observe
378 positive selection of gene Kos. In particular, we confirmed *SOCS1* as the top-scoring gene, followed by
379 *PTPN2* and *REGNASE-1* in third place. (Fig. 8 I) These results are quite consistent to those observed in
380 the subcutaneous tumour, making it difficult to determine whether selection effects are a result of
381 local proliferation or a consequence of CAR-T cell recirculation from the primary lesion. Nonetheless,
382 it is interesting to note that for some genes, notably *REGNASE-1* and *SOCS1*, the results of this
383 screening appear somewhat intermediate between those of the orthotopic tumour model screening,
384 (Fig. 3 D) with the lung as primary tumour site, and the results of the screening in the subcutaneous
385 tumour. (Fig. 8 H)

386 ***Application of the screening assay for the improvement of CAR-T cells mitochondria metabolism,***
387 ***another relevant phenotype in our context***

388 Finally, we wondered if we could apply our approach to study other characteristics of CAR-T cells that
389 may be particularly relevant in a given context, with the aim of integrating these data with the results
390 from the *in vivo* screenings. We had previously demonstrated that CAR-T cell metabolism plays a
391 pivotal role for the efficacy of the therapy in lung tumour model. In particular we could describe that
392 an enhanced mitochondrial respiration could lead to better CAR-T cells migration and ultimately
393 improved tumour control.[76] Therefore, we set up a screening assay in order to select genetic
394 modifications that could improve this parameter. To achieve this, we performed CAR-T cells sorting,
395 selecting respectively the10% of cells with the lowest or the highest staining levels for the standard

396 mitochondrial marker MitoTracker. (Fig. 9 A, B) Then, we indeed verified that cells belonging to the two
397 groups had respectively a lower and higher number of mitochondria. (Fig. 9 C) We then analysed gene
398 KO subpopulations enriched in the highest expression group compared to the lowest, and identified
399 two top-scoring gene, PRDM1 and IRF2, in CAR-T cells from the three donors used. (Fig. 9 D)

400 We therefore produced individual KO CAR-T cells, (Supplementary fig. 8 A) to verify if these modifications
401 could induce an increase in mitochondria abundance. We confirmed this for both genes using
402 MitoTracker staining, (Fig. 9 E) and at the mtDNA level for *PRDM1* KO. However, we detected a large
403 variability of mtDNA quantification for the *IRF2 KO*, which could require further investigation (Fig. 9 F).
404 Nonetheless, we assessed if the KO of these genes could as well increase the respiratory capacity of
405 CAR-T cells. We confirmed a significant increase in respiration for *PRDM1* KO CAR-T cells, whereas no
406 difference was detected for *IRF2* KO. (Fig. 9 G) Finally, we tested if the increased respiratory capacity
407 of *PRDM1* KO CAR-T cells could enhance migration in our 3D motility assay. Indeed, we observed a
408 significant increase in migration for PRDM1 KO, while consistently no difference was detected for *IRF2*
409 KO. (Fig. 9 H)

410 Therefore, we could confirm the efficacy of our screening to determine genes increasing MitoTracker
411 signal. This approach revealed to be a valid strategy to identify promising gene editing modifications
412 that improve mitochondrial mass and ultimately, respiratory capacity. Nonetheless, MitoTracker signal
413 alone does not appear to be a sufficient predictor of these characteristics. Indeed, although both genes
414 identified in the screening exhibited a consistently increased MitoTracker signal, only *PRDM1* KO had
415 a clear effect on respiratory and migratory capacities.
416 On one hand, these results support the versatility of our screening as a tool for broader studies on
417 CAR-T cells. On the other hand, they highlight the importance of combining studies with a pertinent *in*
418 *vivo* screening. Indeed, under our conditions, *PRDM1* KO, while improving CAR-T cells migratory
419 capacities, clearly undermines CAR-T cell persistence and/or proliferation upon restimulation, both *in*
420 *vitro* and *in vivo*, making it an unsuitable target for CAR-T cell amelioration in this context.

421

422 **CONCLUSION**

423 The once unforeseeable successes of CAR-T cells therapy come with the need for further
424 improvements, aiming to achieve remission in all leukaemia and lymphoma patients or extend
425 treatment of solid malignancies.[1] Mainly, the first limitation to tackle, in hematologic malignancies
426 and probably most importantly in solid cancers, appears to be the poor proliferation and/or
427 persistence of CAR-T cells in patients.[2, 4, 32] In this context, several groups gave incredible
428 contributions, proposing ameliorations to the therapy and, among these, gene editing strategies hold
429 great promises.[9, 10]

430 In parallel with the significant effort to discover new strategies, another impelling need should not be
431 neglected; identifying which of these strategies would be most effective in the specific contexts of each
432 CAR-T cell therapy. It is indeed crucial to consider that CAR-T cell therapies being developed worldwide
433 differ largely in several aspects including, the tumour and the antigen targeted, the CAR construct
434 design, the production pipeline and the predicted patients' profiles. These differences have obvious
435 impacts on their efficacy. [19-23]

436 Different whole genome CRISPR-KO approaches have been applied to study T or CAR-T cells
437 amelioration and these studies have allowed to discover effective gene KO strategies in preclinical
438 models. Two key lessons could be learnt by these studies. First, the application of such approaches *in*
439 *vivo* required ingenious strategies and specific settings to overcome the limitations intrinsic to these

models, making it difficult to envision their use for context specific studies. [25, 27-30] The second lesson is that context specific studies may be of great importance, as these investigations could not, or only partially reproduce data one from another. [24-30]

For these reasons, in the present work, we propose a method that aims to serve specifically a comparative analysis, to allow small scale, context specific studies to identify genetic modifications that would be effective for a given CAR-T therapy.
This approach allowed to determine in our study on lung tumour, a shortlist of genes improving CAR-T cells proliferation and or persistence within an orthotopic tumour model, *REGNASE-1, SOCS1, PTPN2* and *P16INK4A*. We performed proof of concept validation that individual KO of 2 of such genes, *REGNASE-1* and *PTPN2* could clearly enhanced CAR-T cell antitumour efficacy. These genes would therefore be a prime target choice in the development of improved CAR-T cells to treat non-small celllung cancer.
Surprisingly we could also determine genes, as *MED12, PRDM1* and *BATF,* whose KO led to negative selection in our screening, coherently through different donors, despite having been described as beneficial in other contexts.[11, 26, 56] Consistently, we could then as well verify that *MED12* KO had a negative impact on tumour control capacities. While these results do not undermine the potential of such genetic modifications *per se*, given the convincing positive effects on CAR-T cells in the context of other studies, surely confirm the need for context specific analyses.

An approach like the one proposed, by allowing to determine genetic modifications with positive and eventually negative effects in each context, could help collecting insights on underlying biological mechanisms of therapeutic success or failure.
We could notably observe for *REGNASE-1* KO CAR-T cells, a marked over-representation of highly activated, pre-exhausted and cytotoxic CD4 and CD8 cells, in the tumour site, which correlated to antitumour efficacy, in our orthotopic lung tumour model. Such increased activation state could explain the markedly improved proliferation of these cells, that does not appear to come to the expenses of cytotoxic proprieties, assuring antitumour efficacy. The upregulation of immunomodulatory markers, seem to not have impacted these qualities and may instead be a consequence of high activation. From this perspective, the phenotype of these cells shares some characteristics of CD8 cells described as Tpex [77],which have been associated with improved persistence of CAR-T cells and better tumour control. Notably, these cells were reported to be enriched in *REGNASE-1* KO CAR-T cells in mice [78].
On the other hand, we could observe an accelerated differentiation of *MED12* KO CAR-T cells during the production phase, which may explain their enhanced proliferation *in vitro* and potentially the improved *in vivo* efficacy observed in other models.[26] However, in this specific context, this accelerated differentiation is ultimately deleterious.

Another critical aspect to consider when studying gene editing strategies for CAR-T cell therapy optimization, is the necessity of employing several models and assays, each addressing different aspects of the therapy. [79, 80] Consequently, CAR-T cells improvement driven by gene modification could benefit from the integration of multiple readouts.

For CAR-T therapy in a given pathology, different *in vivo* models may be valuable, as each can provide different insights, potentially better modelling the actual challenges encountered in patients. The xenografted orthotopic lung tumour for its localisation would allow for a more accurate assessment of key real-life factors such as CAR-T trafficking and tumour growth within a physiologically real-life niche. [81] Conversely, subcutaneous tumour models offer advantages from other points of view, as they allow longer-term studies and constitute a challenging tumour mass for infiltration. These structural

obstacles represent a key aspect in the understanding of CAR-T cell therapeutic failure in tumours and a major subject of interest in the field.[82, 83] In our context, we performed our screening in both models, using the same CAR-T cells and target cell line.
Indeed, comparing screening results from both models provides valuable insights into potential target genes for CAR-T cells amelioration. In our orthotopic lung tumour model, *REGNASE-1* KO appear as a strong candidate for CAR-T cell amelioration, a finding we could as well validate. Nonetheless, *SOCS1* KO scored equally well as *REGNASE-1* KO in this model and significantly outperformed *REGNASE-1 KO* in the subcutaneous model. These data would suggest that differences in the niche, accessibility or the longer timeline of this experiment confer an extra advantage to *SOCS1* KO CAR-T cells. It is difficult to predict if real life conditions in patients would rather resemble completely to the orthotopic model or be better resumed by the subcutaneous model. However, integrating information from both screenings enhances confidence in identifying *SOCS1* KO as a highly promising strategy for CAR-T cells amelioration in this context.

A new exciting area of interest in CAR-T cell research in solid tumours is the role of CAR-T cells in controlling and eliminating metastases. By enabling ubiquitous tumour eradication and enhancing immunosurveillance, CAR-T cells could assure relapse free remission [84, 85]
Here we could perform, in the same mice, a study of CAR-T cells genetic modifications enriched in both primary tumour and metastatic sites. First, we could observe a general concordance among results, either due to concordant independent selection of a similar set of genes or rather to recirculation of CAR-T cells among the two sites. At the same time, it is interesting to note that for KO of genes such as *SOCS1* and *REGNASE-1,* results in the lung as metastatic sites are intermediate within results in the subcutaneous tumour and in the orthotopic lung tumour model. Such effect could be explained by some sort of niche specificities predilection of some CAR-T cells gene editing strategies, and further studies in this direction would be of great interest.

Further addressing the question of context specific readouts, several examples can be made, in some contexts PD-L1 induced inhibition may be a main obstacle, in others it could be nutrients deprivation or hypoxia within the tumour site.[86-88] Specific screenings experiment could be implemented to define gene editing strategies addressing these challenges. Such information could then be used to prioritize genes otherwise scoring similarly in the *in vivo* assay.
In our tumour model, we previously demonstrated the importance of a strong mitochondrial metabolism and migratory capacities of CAR-T cells.[76] We so employed our screening for a test to individuate gene KO strategies that would lead to an improvement in these parameters. We could successfully identify that *PRDM1* KO increases CAR-T cells mitochondrial mass, respiratory capacity and migration. Unfortunately, as we could determine in the other screenings, such gene editing strategy impairs CAR-T cell expansion and persistence. Such result could suggest, as our previous evidence also support, migratory capacity and proliferation may be necessarily competing dynamics.

Results from all these readouts, could also help direct more complex editing approaches, combining different gene KO strategies. It has been shown that KO of genes prioritized in our studies *REGNASE-1*, *PTPN2* and *SOCS1* can be combined with additive effects.[29] Given the current limitations of CAR-T therapy in lung tumour, such a “radical” approach could be taken in consideration. In this work, we also prove the efficacy of a suicide gene approach in eliminating *REGNASE-1* modified CAR-T as well as non-modified ones. Such safety switch system could be fundamental in accompanying the development of these modified CAR-T with hyperproliferative potential, allowing toxicity control.

533 To conclude, we propose a new approach to CRISPR-KO screenings in CAR-T cells, adapting this
534 technology, making it more accessible to allow its application for studying specific CAR-T cells therapies
535 improvement in challenging, but more relevant contexts as specific *in vivo* models. Of interest, a very
536 recent study (preprint [89]) using an approach similar to what described here, but in a model of
537 Multiple Myeloma could also confirm the importance of *REGNASE-1, SOCS1* and *PTPN2,* while not
538 observing either a positive or negative impact of *MED12* inactivation, also included in their gRNAs
539 bank. Such data suggest that some gene inactivation strategies could have an universal efficacy,
540 suggesting a T-cell intrinsic mode of action, even though we could observe quantitative differences of
541 such effects in different models. Others, on the contrary, may be more dependent on other factors,
542 making these strategies ineffective or even deleterious in some conditions, while very effective in
543 others, therefore advocating for the interest in context specific studies on CAR-T cells improvements.

544

545 **MATERIALS AND METHODS**

546

547 ***Study approvals***

548

549 All human studies were conducted in compliance with French regulations on biomedical research and
550 followed the principles outlined in the 1975 Helsinki Declaration and its subsequent revisions.
551 Peripheral blood samples from adult donors were obtained from the Etablissement Français du Sang
552 (EFS) under agreement 18/EFS/030, with informed consent provided for research purposes. These
553 samples were anonymized and were not linked to any personal information, including age, gender, or
554 sex.
555 NOD.Cg-Prkdc^(scid)Il2rg^(tm1Wjll)/SzJ (NSG) immunodeficient mice were acquired from The Jackson
556 Laboratory (Bar Harbor, ME, USA, strain 005557). The animals were housed under pathogen-free
557 conditions at the Cochin Institute Animal Facility, in cages containing no more than 5-6 mice, separated
558 by sex. Environmental conditions, including a 12-hour light/dark cycle, temperature, humidity, and
559 pressure, were maintained according to FELASA guidelines. Cage enrichment included small square
560 houses, cotton, wooden sticks, and paper bedding. Veterinary staff monitored mouse health regularly,
561 and pathogen screening was performed per FELASA standards. Efforts were made to minimize animal
562 discomfort and reduce the number of animals used, adhering to the European Communities Council
563 Directive of 24 November 1986 (86/609/EEC). Mice were included in experiments regardless of sex,
564 ensuring balanced distribution across experimental conditions, and euthanasia was performed via
565 cervical dislocation. The study protocol received approval from Paris Descartes University (CEEA 17-
566 039) and the French Ministry of Research (APAFiS 15076).

567

568 **Cell Culture and Reagents**

569

570 Peripheral blood mononuclear cells (PBMCs) were isolated via Ficoll gradient centrifugation (800 g for
571 20 min, RT) and cryopreserved in a solution of 90% fetal bovine serum (FBS; Thermo Fisher A3840002)
572 and 10% DMSO (Thermo Fisher, 327182500). For CAR-T cell production, PBMCs were cultured in RPMI
573 1640 medium (Thermo Fisher, 21875) supplemented with 10% FBS, 2 mM L-glutamine (Thermo Fisher,
574 25030081), and 100 U/ml penicillin/streptomycin (Thermo Fisher, 15140130), with the addition of 25
575 ng/ml IL-7 and IL-15 (Miltenyi, 130-095-363 and 130-095-765). Cells were activated 24 hours post-thaw
576 using T cell TransAct (Miltenyi 130-111-160) at a 1:200 dilution for 48 to 96 hours, depending on the
577 experiment. Following activation, the culture medium was completely replaced, and cells were
578 maintained with cytokine supplementation alone.

For experiments involving the sgRNA-expressing lentiviral library, individual sgRNA-expressing viruses, or the iCasp9-expressing virus, puromycin (Thermo Fisher, A11138-03) was added at 1 µg/ml two days post-nucleofection for three days, after which the concentration was reduced to 0.5 µg/ml and maintained for the remainder of the culture period. Human A549 (mCherry$^+$ and Luciferase$^+$) and HEK-293T tumour cells (from in-house stocks) were cultured in DMEM medium (Thermo Fisher, 11995) with the same supplements used for RPMI-based T cell cultures. All cell lines were routinely tested for mycoplasma contamination.

T cells viral transduction and gene editing

For experiment the sgRNA expressing lentiviral bank or individual sgRNA expressing viruses the following procedure was followed. Cells are infected at 24h with 2.5 ul/ml of medium of lentiviral pool expressing sgRNAs or lentiviruses expressing individual sgRNAs. At 48h medium is changed and cells are infected with 100ul/ml of CAR-expressing viruses, with addition of lentiBOOST (Revvity SB-A-LF-901-01) at 1:200 concentration. At 72h medium is changed, cells are washed, divided in 5 × 105 aliquots, resuspended in 16.4 µl P3 and 3.6 µl Supplement Reaction solutions from P3 Primary Cell 4D X Kit S (Lonza V4XP-3032) and 5 ug of Cas9 protein (Thermo Fisher A36497). Electroporation was performed using Amaxa 4D Nucleofector (Lonza), following the manufacturer instruction. After 30 min recovering at 37 °C, cells were put back in culture under stimulation conditions for an additional 24 h. In procedures involving no gene editing, the simple CAR virus infection is performed. In the suicide gene experiment, cells were infected at 24h with 100ul/ml of i*CASP9*-expressing viruses, at 48h are infected with the CAR-expressing virus, and at 72h sgRNAs (Thermo Fisher A35534) in a molar proportion of 3 to 1 to the Cas9 protein are added during the nucleofection step. *REGNASE-1* sgRNA used for RNP editing procedure had target sequences 5'-AAGGAGGTCTTCTCCTGCCG-3' and 5'-CAGTGTTTGTHCCATCCTGG-3' [69]

Lentiviruses design and production

To generate anti-EGFR 41BB-CAR, downstream of a signal peptide scFv sequences derived from nimotuzumab Ab (IMGT/2Dstructure-DB INN 8545H, 8545 L) were introduced into the expression cassette encoding CD8 hinge and transmembrane domains (194–248 Aa, GenBank: AAH25715.1), 4-1BB costimulatory domain (214-255 Aa, GenBank: AAX42660.1), CD3z signaling domain (52-163 Aa, GenBank: NP_000725.1) and GFP coding sequence (downstream of IRES sequence).

To generate anti-EGFR CD28-CAR, 41BB sequence was replaced with CD28 sequence (GenBank: NM_001243078.2), all the remaining sequence was conserved, in a new vector (Vector builder VB240303-1098rav)

Lentivirus expressing FK506-binding protein 12 (with F36V mutation) fused with human caspase-9 protein deleted for 1-134 AA and linked to a HA tag, was purchased as already commercially available (Vector Builder VB900176-7377zdg).

Lentiviral bank expressing gRNAs (Vector builder Lib230420-1523hhp) was designed on demand by vector builder by inserting custom sgRNAs in the company commercially available sgRNA expression plasmid. To design the bank, 50 genes of interest were targeted, along with 4 essential genes of T-cells activation pathway used as negative control (LCP2, RHOH, VAV1, ZAP70). For each gene 4 gRNAs were designed, including, when possible, at best 2 gRNAs previously described in the literature. 20 non-targeting gRNAs were also added as baseline control.

All sgRNA expressing plasmids were also designed on demand starting from the same sequence, with custom sgRNA expressing region: sgRNA targeting *EGFP* (Vector builder VB230314-1357xnw sgRNA sequence: 5'-GGGCGAGGAGCTGTTCACCG-3'), sgRNA targeting *RINF* (Vector builder VB230314-1123mnq, sgRNA sequence: 5'- GTTGCTTTTGTCCACCGCCA-3'), sgRNA scramble (Vector builder VB240125-1049dfy sgRNA sequence: 5'-ACGTGGGGACATATACGTGT-3'), sgRNA targeting *REGNASE-1*(Vector builder VB240125-1038zad, sgRNA sequence: 5'-TTCACACCATCACGACGCGT-3'), sgRNA targeting *PTPN2*(Vector builder VB240216-1035aey, sgRNA sequence: 5'-AGTGCAGGCATTGGGCGCTC-3'), sgRNA targeting *MED12*(Vector builder VB240715-1614nfg, sgRNA sequence: 5'-TAACCAGCCTGCTGTCTCTG-3'), sgRNA targeting *PRDM1*(Vector builder VB240918-1470wdv, sgRNA sequence: 5'-TCGATGACTTTAGAAGACGT-3') and sgRNA targeting *IRF2* (Vector builder VB240918-1473bwg, sgRNA sequence: 5'-GGATGCATGCGGCTAGACAT-3').

Production of lentiviral particles was performed by transient co-transfection (polyethylenimine:DNA at 3.5:1 ratio) of HEK 293 T cells with plasmids expressing the sequence of interest and second-generation packaging system plasmid psPAX2 and pMD2.G (Addgene, 12260 and 12259). Viral supernatants were harvested at 48 and 72 h post-transfection. Viral particles were concentrated by ultracentrifugation at 25.000 g for 2 h and conserved at −80 °C.

Gene editing assessment by deconvolution assays

DNA extraction from bulk edited and ctrl CAR-T cells was performed with FastPure Blood/Cell/Tissue/Bacteria DNA Isolation Mini Kit (Vazyme DC112-01-AB). Cells were lysed in the presence of proteinase-K (Vazyme, DE102-01) at 56°C, then DNA was isolated by silica gel columns purification technology. We assessed gene editing efficiency by amplifying the genomic region encompassing the CRISPR-Cas9 sgRNA target site using PCR with primers flanking this region. The PCR amplicons were then subjected to Sanger sequencing with Eurofins tubeSeq supreme service. To analyse the sequencing data, we utilized the Deconvolution of Complex DNA Repair, DECODR (ChristianaCare) [90] accessible via the Latch.bio online console (LatchBio). DECODR employs a deconvolution algorithm to interpret mixed sequencing chromatograms, enabling the quantification of indel frequencies and the identification of mutated sequences within DNA from bulk cells population.

Orthotopic and subcutaneous tumour models

For the orthotopic tumour model, 4 × 106 human A549 cells (mCherry+ Luciferase+) were injected i.v. into the tail vein of 6 to 10 weeks-old NSG nude mice (independently of sex, respecting uniform sexes proportions in different conditions groups) in most of the experiments. in a single screening experiment, 20 x 106 A549 cells were injected instead.
For the tumour infiltration assessment after 3 weeks, mice were infused i.v. with 5 × 106 anti-EGFR CAR T cells into the tail vein. After 4 days, mice were sacrificed, and lungs were collected.
For in vivo tumour exposure experiments, and tumour growth follow up, 3 days after i.v. injection of A549 cells, mice were injected i.v. with anti-EGFR CAR T cells into the tail vein, numbers of CAR-T cells in different experiments and are specified in the text. Tumour growth in the lungs was followed by bioluminescence using PhotonIMAGER system (Biospacelab) and analysis was performed using M3Vision software (Biospacelab, software version 1.2.1.32016). To assess tumour burden in the orthotopic model, an evaluation grid was implemented according to our ethical committee in order to sacrifice mice reaching a defined endpoint threshold (calculated by taking into account tumour

673 bioluminescence score, mouse behaviour, physical appearance, weight, etc.). Mice were sacrificed as
674 soon as reaching the endpoint threshold score.
675 For the subcutaneous tumour model, 5 × 106 human A549 cells were injected s.c. into the right flank
676 of 2 months-old NSG nude mice (independently of sex, respecting uniform sexes proportions in
677 different conditions groups). To evaluate CAR T cell infiltration, mice were injected i.v. after 5/6 weeks
678 with 5 × 106 anti-EGFR CAR T cells and sacrificed 4 days after to perform the same analyses described
679 for orthotopic tumours. Alternatively, 14 days after A549 cell injection, A549-derived tumour-bearing
680 mice were i.v. inoculated with 7 × 106 anti-EGFR CAR T cells or 5 × 106 anti-EGFR CAR T modified with
681 the lentiviral bank and tumour growth was followed through caliper measurement for additional 9-11
682 weeks. An evaluation grid was designed for this model too, with adapted criteria for caliper
683 measurement of tumour mass, mice were sacrificed as soon as reaching the endpoint threshold score.
684
685 ***Immunofluorescence on tissue samples***
686
687 Lung or subcutaneous tumour samples were fixed o.n. with PLP solution (1% paraformaldehyde, 2 mM
688 lysine-HCl, 550 mg/L NaIO4) at 4 °C, cut into 1–2 mm3 pieces, embedded into 7% agarose (Sigma
689 Aldrich A0701) and then cut into 150 µm-thick sections through vibratome (VT 1000 S, Leica). For
690 extracellular staining, slices were incubated 1 h at RT with 0.5% BSA in DPBS. Then, slices were placed
691 onto Millicell 0.4 µm organotypic insert (Millipore PICMORG50) and 30 µl of 0.5% BSA / DPBS solution
692 (for extracellular staining) containing the desired Abs were added. A metal ring was used to keep the
693 solution in place on the slice. Abs were incubated o.n. at 4 °C. The day after, slices were washed twice
694 in DPBS and then mounted using Superfrost microscope slides (Epredia J1800AMNZ) and Vectashield
695 antifade mounting medium (VectorLabs H-1900). The following antibodies were used (200 ng/slice):
696 FITC-anti-CD3 (Biolegend 344804, clone SK7), PE-anti-EpCAM (Biolegend 324206, clone 9C4). 4',6-
697 Diamidino-2-phenylindole at the concentration of 1/1000 was used to stain for all cells nuclei. Images
698 were acquired using a spinning-disk (Yokogawa CSU-W1 T1) Ixplore IX83 microscope (Olympus)
699 equipped with ORCA-Flash 4.0 V3 (sCMOS Hamamatsu) camera and CellSens Dimension software
700 (Olympus, v4.1.1). To analyse protein expression in NSCLC samples, an ImageJ threshold mask was
701 used to identify EpCAM+ areas (tumour islets) and T cells. Then, "subtract" or "multiply" ImageJ
702 commands were used to define T cells in tumour stroma or islets, respectively. Protein expression
703 (MFI) was calculated in the selected T cell populations.
704
705 ***HES staining on tissue samples***
706
707 The tissues are fixed in 4% PFA for 24 hours, then dehydrated in a graded ethanol series, isopropanol,
708 and xylene (Thermo Fisher, A11358.0F) before impregnation and embedding in paraffin for storage as
709 FFPE blocks. The tissues are sectioned into 4 µm thick slices using a microtome (Autosection, Sakura).
710 The slides are stained automatically on the SPECTRA stainer (Leica) using H&E. They are deparaffinized,
711 rehydrated, rinsed, incubated for 3 minutes in Mayer's haematoxylin, rinsed again, stained for 5
712 minutes in erythrosine, followed by 5 minutes in 1% alcoholic saffron. The stained slides were scanned
713 at 20x magnification using the Lamina Slide Scanner (Perkin Elmer) and analysed with the Case Viewer
714 software (v 2.2).
715
716 ***Tumours and organs dissociation***
717
718 For flow cytometry and DNA extraction, tumour bearing mice lungs were cut to 1-2 mm length pieces,
719 then digested with Liberase (Roche 5401119001) solution at 37 °C for 30 minutes and then smashed
720 using a 70 µm Cell Strainer filter (Corning 352350). Collected cells were either stained with Abs for flow

721 cytometry analysis (BD Fortessa), or pelleted and frozen for DNA extraction. Subcutaneous Tumours
722 were treated as described above for lungs in order to obtain single cells suspension, cells were also
723 either stained with antibodies or pelleted and frozen for DNA extraction. Mice spleens were also
724 collected and directly smashed using a 70 µm Cell Strainer filter (Corning 352350), cells were then used
725 as described above.
726
727 ***Tumour infiltrating CAR-T cells isolation***
728
729 For experiments characterising effects of tumour exposure on CAR-T cells, such cells were isolated
730 from single-cell suspensions using the human CD45 MicroBead Kit (Miltenyi, 130-121-563) and LS
731 Columns (Miltenyi, 130-042-401). Cells were resuspended in MACS buffer, incubated with CD45.1
732 MicroBeads at 4°C for 15 minutes, washed, and centrifuged at 300 × g for 5 minutes. The labelled cells
733 were applied to LS Columns in a magnetic separator, washed, and eluted by flushing with buffer.
734 Collected CAR-T cells were either stained for flow cytometry (BD Fortessa) phenotyping, for lung
735 tumour characterisation experiment, or put back to culture for 48 hours and consequently used in
736 cytotoxicity and proliferation experiments, for both lung tumour and subcutaneous tumour
737 characterisation experiments.
738
739 ***Cytotoxicity assays***
740
741 The cytotoxic activity of in vitro expanded and tumour-derived anti-EGFR 41BB-CAR T cells was
742 assessed using mCherry-expressing A549 cells. Briefly, A549 cells were seeded at a density of 20×10^5
743 cells per 250 µl in 96-well plates (Corning 351172) using DMEM medium. After 48 hours (defined as
744 time 0 h), anti-EGFR 41BB-CAR T cells were introduced at a CAR:target ratio of 3:1 in RPMI complete
745 medium, without supplementary cytokines. A549 cell viability was determined by measuring the
746 mCherry-positive area at various time points. In the experiment shown in Figure 2, fluorescence
747 microscopy was used, while all other experiments employed an Incucyte S3 (Sartorius). The mCherry-
748 positive area was compared between wells with and without CAR T cells to evaluate cytotoxic effects.
749
750 ***In vitro proliferation assays***
751
752 *In vitro* cultured and tumour isolated Anti-EGFR 41BB-CAR T cell proliferation capacity have been
753 evaluated by trypan blue corrected living cell counting. Cells were put in culture for 48h hours in
754 complete T cells culture medium, then were stimulated with anti-CD3/CD28 conjugated colloidal
755 polymer T cells TransAct (Miltenyi, 130-111-160) at 1:200 concentration for 48 hours. Cells
756 proliferation was followed for 7 days after activation.
757
758 ***Flow cytometry***
759
760 FSC-A/SSC-A gating and LIVE/DEAD™ Fixable Blue Dead Cell Stain Kit (Invitrogen, L23105) have been
761 used to define live and dead cells. The following antibodies have been used to stain extracellular
762 proteins (1:100 dilution): BV785 CD45 (Biolegend, 304048), PE CD45 (Biolegend, 368509), BV650 CD4
763 (Biolegend, 317436), BUV737 CD8 (BD Biosciences, 612754), BV711 anti-CD45RA (Biolegend 304138),
764 APC anti-CD45RO (Biolegend, 304210), APC-Cy7 anti-CD27 (Biolegend, 302816), PE-Cy7 anti-CCR7
765 (Biolegend, 353225), APC anti-PD-1 (Miltenyi, REA1165), BV421 TIM3 (Biolegend, 345007), BV786
766 LAG3 (Biolegend, 369321), PE-Cy7 anti-CCR7 (Biolegend, 372713). For T cell subpopulations, the
767 following subsets were defined by flow cytometry gating strategy: stem cell memory-like (Tscm,
768 CD45ROnegCCR7pos or CD45RAposCD27pos); effector-like (Teff, CD45ROnegCCR7neg or

769 CD45RAposCD27neg); central memory-like (Tcm, CD45ROposCCR7pos or CD45RAnegCD27pos);
770 effector memory-like (Tem, CD45ROposCCR7neg or CD45RAnegCD27neg).
771 To evaluate Anti-EGFR 41BB-CAR or sgRNA expression in transduced cells, fluorescence signal of
772 respective reporter genes in the vectors, GFP and mCherry, was analysed.
773 To evaluate mitochondrial mass cells were incubated for 20/30 min at 37 °C in the presence of 10 nM
774 MitoTracker Deep Red (Thermo Fisher M22426). Then, cells have been washed and analysed. Samples
775 were analysed using BD Fortessa (FACSDiva software v6.1.3).
776
777 ***Correlation study on bioluminescence and infiltrating CAR-T cells % data***
778
779 At the endpoint of the experiment, data on tumour charge assessed by bioluminescence and
780 abundance of CAR-T cells determined by flow cytometry were used for statistical analysis aiming at
781 establishing the presence, if any, of a direct or inverse correlation between the two variables. A
782 confidence interval for the measured tumour charge at every point can be used to statistically assess
783 the goodness of fit, and in our case, it is defined as the standard deviation of the photon rate (oscillating
784 during the measurement). After trying a few simple models, the best-performing one, assessed by log-
785 likelihood maximization, was a power law of the following form:
786 $$\boldsymbol{Y = A * X^{B}},$$
787 where the best-fitting parameters were estimated as $\boldsymbol{A = 4.8 * 10^{6}}$ and $\boldsymbol{B = -8.6 * 10^{-1}}$. The
788 optimization was executed by assuming a gaussian-like noise on the data, in order not to penalize data-
789 points with significantly greater error-bars. This is a wide-spread convention for counting experiments
790 in other fields as well and is well justified.[91]No systematic error in the taken measurements was
791 considered for this study.
792
793 ***SgRNA readout by deep sequencing***
794
795 The sgRNA library readout was performed using a PCR amplicon sequencing strategy, where a PCR on
796 sample genomic DNA is performed, with adapters P5 and P7 bound custom primers (Eurofins) targeting
797 a 350 bp vector region including the sgRNAs cassette.
798 Adapter-Forward: ACACTCTTTCCCTACACGACGCTCTTCCGATCT-TTGCATATACGATACAAGGCTGT
799 Adapter-Reverse: GACTGGAGTTCAGACGTGTGCTCTTCCGATCT-ACAAAGTTGGAATTCGGTACCTC

800 PCR was performed using Platinum™ SuperFi II PCR Master Mix (ThermoFisher, 12368010), with
801 addition of 5% DMSO. the thermocycling parameters were: 98°C for 8min, 35 cycles of (98°C for 30 s,
802 58°C for 30 s, 72°C for 1 min), and 72°C for 10 minutes. In each PCR reaction, 2 µg of total gDNA were
803 used. For each sample, 3 independent PCR reactions were performed.
804 PCR products from each sample were pooled and gel purified using a 2% agarose (Sigma Aldrich A0701)
805 gel and FastPure Gel DNA Extraction Mini Kit (Vazyme DC301-01) then normalized before shipping to
806 Eurofins Genomic, where samples were sequenced according to the commercially available procedure
807 NGSelect Amplicon illumina Miseq, (Eurofins genomics) producing 60K double-stranded reads per
808 sample. The service includes basic quality control trimming of FASTQ files.
809
810 ***MAGeCK analysis of gene KO subpopulations enrichment***
811
812 For MAGeCK analysis, FASTQ files were used as inputs to create count tables using to the MAGeCK -
813 count algorithm a command-prompt based tool (https://sourceforge.net/p/MAGeCK/wiki/Home/).
814 The count tables were then used as input for MAGeCK -test algorithm. In such algorithm, "mean"
815 setting was used to calculate LFC, normalization method was set to "total" and a list of non-targeting

control sgRNAs provided for normalization and generation of the null distribution of RRA, with the exception of analyses on subcutaneous tumour samples and lung samples from this experiment. In these experiments all gRNAs were used for normalization; due to the extremality of data in these experiments, such approach confers a more conservative but more effective calculation of p-values. All LFC data plotted are corrected to the mean LFC of the non-targeting gRNAs, all sum of ranks use ranking from MAGeCK RRA algorithm, with the exception of analyses on subcutaneous tumour samples and lung samples this experiment. In this case, an LFC based ranking was used instead, allowing to correct for biases due to extremality of data. p-values and FDR values indicated for screening experiments are reported as calculated by the MAGeCK algorithm.

Inducible cell death experiment

i*CASP9* expressing CAR-T cells were stimulated with anti-CD3/CD28 conjugated colloidal polymer T cells TransAct (Miltenyi, 130-111-160) at 1:200 concentration for 48 hours. Then medium was changed, and cells were re-seeded at 1x106 cells/ml concentration, and AP20187 (MedChemExpress HY-13992) resuspended in DMSO for a final concentration of 5 nM or simply DMSO vehicle were added. Cell survival at different time points was assessed as % of living cells as determined by Fixable Live dead blue (Thermofisher, L23105) staining, corrected for the actual number of cells where a reduction in detectable cells compared to time 0 was observed.

CytOF staining and data analysis

Frozen samples were thawed and washed in phosphate-buffered saline (PBS) supplemented with 0.5% (w/v) bovine serum albumin (BSA; Sigma-Aldrich, A7030), 0.02% (v/v) sodium azide, and deoxyribonuclease (15 µg/mL). Cells were stained with a surface antibody cocktail in PBS containing 0.5% BSA and 0.02% sodium azide at room temperature (RT) for 15 minutes (see Supplementary Table X for antibody clones, references, and metal conjugates).
For viability staining, cells were incubated with 5 µM cisplatin in PBS for 5 minutes, as previously described.[92] After two washing steps, cells were permeabilized using Cyto-Fast Fix/Perm Solution (BioLegend, 750000133) for 30 minutes at RT. Following permeabilization, cells were washed with permeabilization buffer and stained intracellularly with anti-Perforin, anti-Granzyme A, anti-Granzyme B, anti-Granzyme K, and anti-CTLA-4 antibodies for 30 minutes at RT in permeabilization buffer. After two additional washes, cells were fixed in PBS containing 2% paraformaldehyde (PFA) overnight. DNA staining was performed as previously described.[93]
Purified antibodies devoid of carrier proteins were obtained from the suppliers listed in (Supplementary tab. 1). Antibody conjugation was performed following the protocol provided by Standard Biotools. CyTOF acquisition was conducted as previously described [92] To account for zero values in the dataset, values of zero were randomized using a uniform distribution between zero and minus one via a custom R script, consistent with previous CyTOF software defaults. All other integer values measured by the mass cytometer were similarly randomized by default.
For UMAP analysis, data processing was performed using custom R scripts based on the "flowCore" and "uwot" packages, following the methodology previously described [94]). Data transformation was applied using the "logicleTransform" function from the "flowCore" package with the following parameters: w = 0.25, t = 16,409, m = 4.5, a = 0, to approximate the scaling historically used in FlowJo. For heatmap visualization, median intensity values were transformed using a logical data scale, following the approach described by Moore and Parks[95]. A four-color scale was applied: black–blue for low expression values, green–yellow for intermediate expression, and red for high expression levels of a given marker within a cluster.

In vitro restimulation assays

For *in vitro* screening restimulation assays, 5x105 Human A549 (mCherry^{pos} and Luciferase^{pos}) were seeded in 12-well plate dishes (corning, 351143). 24 hours plates were irradiated with a dose of 50 Gy with a BIOBEAM GM 2000 machine (Ekert and Ziegler), medium was changed to aforementioned Human T cell medium without added interleukins and CAR-T cells modified with the lentiviral bank were added at a 2:1 Effector to target ratio. For the heavy in vitro restimulation assay, cocultures were renewed every 5 days, with medium change every 3 to 5 days, for a total of 35 days. For the mild in vitro restimulation assay, cocultures were renewed every 10 days, for a total of 35 days. For the 14 days proliferation assays under chronic stimulation, the same CAR-T cells used in the heavy in vitro restimulation assay were cultured in parallel in absence of tumour cells and were restimulated every 5 days with anti-CD3/CD28 conjugated colloidal polymer T cells TransAct (Miltenyi 130-111-160) at 1:200 concentration for 48 hours. At 14 days cells were taken for DNA extraction and compared to cells from the heavy in vitro restimulated assay isolated at 14 days.

Machine learning metastatic burden quantification

We prepared cropped sections of 4.5X magnifications of 20x magnification images obtained from paraffin embedded, HES-stained lung slices acquired through an optical microscope. Such images were processed using InForm® software. To begin, the images were converted to optical density, 2 spectres images with the Eosin and purple haematoxylin channels.
Tissue segmentation was then performed by subdividing images in no-tissue regions, healthy tissue and tumour tissue. At least 10 areas for each category were used to train the machine learning software. Segmentation was then performed automatically by the algorithm, and each image was visually inspected, and segmentation corrected by hand. % of metastatic area was then calculated as % ratio of % metastatic area in each slide / (% of healthy tissue + % of tumour tissue).

Flow Cytometric Sorting of High and Low MitoTracker Red-Expressing Cells

For sorting experiment based on mitochondrial mass, cells were incubated for 20/30 min at 37 °C in the presence of 10 nM MitoTracker Deep Red (Thermo Fisher M22426). Then, cells have been washed and resuspended in sorting buffer (PBS with 2% FBS and 1 mM EDTA).
Cell sorting was performed on a BD FACSAria™ III (BD Biosciences), Forward scatter (FSC) and side scatter (SSC) parameters were adjusted to exclude debris and doublets. Cells were gated based on fluorescence intensity, and the highest 10% (MitoTracker-High) and lowest 10% (MitoTracker-Low) populations were sorted directly into collection tubes containing RPMI-1640 supplemented with 20% FBS. Sorted cells were pelleted and frozen, for subsequent DNA extraction to allow gene-KO subpopulation frequency analysis as previously described.

mtDNA quantification by qRT-PCR

Genomic DNA was extracted using the FastPure Blood/Cell/Tissue/Bacteria DNA Isolation Mini Kit (Vazyme Biotech, DC112-01) following the manufacturer's instructions. Cells were lysed with Proteinase K (Vazyme, DE102-01) at 56°C, and DNA was purified using silica-based column technology.

912 Quantitative real-time PCR (qRT-PCR) was performed using the LightCycler® 480 SYBR Green I Master
913 detection kit (Roche, 04707516001) on a LightCycler® 480 system (Roche) with three technical
914 replicates per sample. Fluorescence signal acquisition and curve analysis were carried out using
915 LightCycler® 480 Software (version 1.5.1.62, Roche). The following primers were used: ND1-Fw 5'-
916 CCCTACTTCTAACCTCCCTGTTCTTAT-3', ND1-Rv 5'-CATAGGAGGTGTATGAGTTGGTCGTA-3', ND5-Fw 5'-
917 ATTTTATTTCTCCAACATACTCGGATT-3', ND5-Rv 5'-GGGCAGGTTTTGGCTCGTA-3', 18S-Fw 5'-
918 AGTCGGAGGTTCGAAGACGAT-3', 18S-Rv 5'-GCGGGTCATGGGAATAACG-3'. Relative mitochondrial DNA
919 levels were calculated using the ΔΔCt method with 18S rRNA as the reference gene.
920
921 ***In vitro motility assay with collagen gel and Analysis of T cell motility***
922
923 T cells were washed once with DPBS, stained with 100 nM of Calcein Green (Invitrogen C34852) or
924 Calcein Red Orange (Invitrogen C34851) for 20 min at 37 °C in DPBS, washed once in motility medium,
925 resuspended in 50 µl at a final concentration of 20 × 106cells/ml and then mixed with 100 µl of collagen
926 solution (PureCol Bovine Collagen, CellSystem 5005, previously neutralized using DPBS 10x) to reach a
927 final collagen concentration of 2 mg/ml. Then, the mixture was loaded into an ibiTreat µ-Slide VI 0.4
928 slide (Ibidi 80606), which was placed at 37 °C in the incubator for 1 h to allow collagen polymerization.
929 Live recording of T cell motility was performed using a Nikon epifluorescence microscope equipped
930 with 37 °C heated-chamber, ORCA-Flash 4.0 camera (C11440 Hamamatsu) and Metamorph software
931 (version 7.10.2.240, Molecular Devices). For each condition, 15 images (30 s time interval, 4/5 z-planes,
932 z-distance 15 µm) were acquired using a 20x objective (binning rate, 2) at 3 different stages. In most
933 cases, T cells from two different donors were stained with Calcein Green and Calcein Red and mixed
934 before adding them to collagen.
935 T cell motility was analysed using ImageJ plugin TrackMate78 (v.7.11.1) in a 3D environment (z-stack
936 distance, 15 µm). LoG detector was used to identify spots (quality and maximal intensity filters applied
937 for collagen assays) and Simple LAP Tracker to identify tracks (linking max distance 20 µm, closing-gap
938 max distance 20 µm, frame gap 3). Only tracks containing 10 or more spots were considered for
939 analysis. Motility Score was calculated as follows: (% of cells moving more than 10 µm as Euclidean
940 distance)*(mean speed [µm/min] of moving cells). Images and movies shown throughout the
941 manuscript are 2D z-stack reconstruction while analyses were performed on original 3D images (i.e.,
942 also taking into account the z-axis displacement).
943
944 ***High-resolution respirometry with Oroboros device***
945
946 The oxygen consumption rate (OCR) was measured in the motility medium (see above) by a high-
947 resolution 2 mL glass chamber Oxygraph-2k respirometer (Oroboros). The electrode was calibrated at
948 37 °C, 100% and 0% oxygen before adding CD8+ T cells (2 mL at 2.5 × 106 cells /mL) to each chamber
949 and the flux of O2 consumption was measured in pmol/s. Oligomycin (0.5 µg/mL) was added to block
950 complex V, as an estimate of the contribution of mitochondrial leakage to overall cellular respiration.
951 Increasing amounts of carbonyl cyanide m-chlorophenyl hydrazone (CCCP) were added to measure
952 maximum respiratory capacity. Finally, potassium cyanide (KCN) was added to measure the non-
953 mitochondrial respiration.
954
955 ***Statistical analysis***
956
957 In the figure legends, "n" represents the number of biologically independent samples, donors, movies
958 analysed in migration assays, or the number of mice used. Data are presented as mean ± SEM or as
959 box-and-whisker plots. Statistical comparisons between normally distributed groups were conducted

using paired or unpaired two-tailed Student's t-test (for two-group comparisons) or One-way and Two-way ANOVA. When normality assumptions were not met, the Wilcoxon Signed Rank Test (for paired data) or ANOVA on Ranks was applied. Pairwise comparisons were adjusted using appropriate post hoc tests. Statistical analyses were carried out using GraphPad (v8).

REFERENCES

1. Cappell, K.M. and J.N. Kochenderfer, *Long-term outcomes following CAR T cell therapy: what we know so far*. Nat Rev Clin Oncol, 2023. **20**(6): p. 359-371.
2. Fraietta, J.A., et al., *Determinants of response and resistance to CD19 chimeric antigen receptor (CAR) T cell therapy of chronic lymphocytic leukemia*. Nature Medicine, 2018. **24**(5): p. 563-571.
3. O'Rourke, D.M., et al., *A single dose of peripherally infused EGFRvIII-directed CAR T cells mediates antigen loss and induces adaptive resistance in patients with recurrent glioblastoma*. Sci Transl Med, 2017. **9**(399).
4. Albelda, S.M., *CAR T cell therapy for patients with solid tumours: key lessons to learn and unlearn*. Nat Rev Clin Oncol, 2024. **21**(1): p. 47-66.
5. Louis, C.U., et al., *Antitumor activity and long-term fate of chimeric antigen receptor-positive T cells in patients with neuroblastoma*. Blood, 2011. **118**(23): p. 6050-6.
6. Del Bufalo, F., et al., *GD2-CART01 for Relapsed or Refractory High-Risk Neuroblastoma*. N Engl J Med, 2023. **388**(14): p. 1284-1295.
7. Brown, C.E., et al., *Locoregional delivery of IL-13Rα2-targeting CAR-T cells in recurrent high-grade glioma: a phase 1 trial*. Nature Medicine, 2024. **30**(4): p. 1001-1012.
8. Sterner, R.C. and R.M. Sterner, *CAR-T cell therapy: current limitations and potential strategies*. Blood Cancer J, 2021. **11**(4): p. 69.
9. Tian, Y., et al., *Gene modification strategies for next-generation CAR T cells against solid cancers*. J Hematol Oncol, 2020. **13**(1): p. 54.
10. Dimitri, A., F. Herbst, and J.A. Fraietta, *Engineering the next-generation of CAR T-cells with CRISPR-Cas9 gene editing*. Molecular Cancer, 2022. **21**(1).
11. Zhang, X., et al., *Depletion of BATF in CAR-T cells enhances antitumor activity by inducing resistance against exhaustion and formation of central memory cells*. Cancer Cell, 2022. **40**(11): p. 1407-1422 e7.
12. Zou, Y., et al., *IKZF3 deficiency potentiates chimeric antigen receptor T cells targeting solid tumors*. Cancer Letters, 2022. **524**: p. 121-130.
13. Prinzing, B., et al., *Deleting DNMT3A in CAR T cells prevents exhaustion and enhances antitumor activity*. Science Translational Medicine, 2021. **13**(620).
14. Fraietta, J.A., et al., *Disruption of TET2 promotes the therapeutic efficacy of CD19-targeted T cells*. Nature, 2018. **558**(7709): p. 307-312.
15. Sutra Del Galy, A., et al., *In vivo genome-wide CRISPR screens identify SOCS1 as intrinsic checkpoint of CD4 + TH 1 cell response*. Science Immunology, 2021. **6**(66).
16. Jung, I.-Y., et al., *CRISPR/Cas9-Mediated Knockout of DGK Improves Antitumor Activities of Human T Cells*. Cancer Research, 2018. **78**(16): p. 4692-4703.
17. Jafarzadeh, L., et al., *Targeted knockdown of Tim3 by short hairpin RNAs improves the function of anti-mesothelin CAR T cells*. Molecular Immunology, 2021. **139**: p. 1-9.
18. Rupp, L.J., et al., *CRISPR/Cas9-mediated PD-1 disruption enhances anti-tumor efficacy of human chimeric antigen receptor T cells*. Sci Rep, 2017. **7**(1): p. 737.
19. Mao, R., W. Kong, and Y. He, *The affinity of antigen-binding domain on the antitumor efficacy of CAR T cells: Moderate is better*. Frontiers in Immunology, 2022. **13**.
20. Weinkove, R., et al., *Selecting costimulatory domains for chimeric antigen receptors: functional and clinical considerations*. Clinical & Translational Immunology, 2019. **8**(5): p. e1049.

1011 21. Wei, J., et al., *Target selection for CAR-T therapy*. Journal of Hematology & Oncology,
1012 2019. **12**(1).
1013 22. Watanabe, N., F. Mo, and M.K. McKenna, *Impact of Manufacturing Procedures on CAR T*
1014 *Cell Functionality*. Frontiers in Immunology, 2022. **13**.
1015 23. Jaeger-Ruckstuhl, C.A., et al., *Phase I Study of ROR1-Specific CAR-T Cells in Advanced*
1016 *Hematopoietic and Epithelial Malignancies*. Clinical Cancer Research, 2025. **31**(3): p.
1017 503-514.
1018 24. Shifrut, E., et al., *Genome-wide CRISPR Screens in Primary Human T Cells Reveal Key*
1019 *Regulators of Immune Function*. Cell, 2018. **175**(7): p. 1958-1971.e15.
1020 25. Dong, M.B., et al., *Systematic Immunotherapy Target Discovery Using Genome-Scale*
1021 *In Vivo CRISPR Screens in CD8 T Cells*. Cell, 2019. **178**(5): p. 1189-1204.e23.
1022 26. Freitas, K.A., et al., *Enhanced T cell effector activity by targeting the Mediator kinase*
1023 *module*. Science, 2022. **378**(6620): p. eabn5647.
1024 27. Zhao, H., et al., *Genome-wide fitness gene identification reveals Roquin as a potent*
1025 *suppressor of CD8 T cell expansion and anti-tumor immunity*. Cell Reports, 2021. **37**(10):
1026 p. 110083.
1027 28. LaFleur, M.W., et al., *A CRISPR-Cas9 delivery system for in vivo screening of genes in the*
1028 *immune system*. Nature Communications, 2019. **10**(1).
1029 29. Wei, J., et al., *Targeting REGNASE-1 programs long-lived effector T cells for cancer*
1030 *therapy*. Nature, 2019. **576**(7787): p. 471-476.
1031 30. Chen, Z., et al., *In vivo CD8+ T cell CRISPR screening reveals control by Fli1 in infection*
1032 *and cancer*. Cell, 2021. **184**(5): p. 1262-1280.e22.
1033 31. Belk, J.A., et al., *Genome-wide CRISPR screens of T cell exhaustion identify chromatin*
1034 *remodeling factors that limit T cell persistence*. Cancer Cell, 2022. **40**(7): p. 768-786 e7.
1035 32. Marofi, F., et al., *CAR T cells in solid tumors: challenges and opportunities*. Stem Cell
1036 Research & Therapy, 2021. **12**(1).
1037 33. Qu, J., et al., *Chimeric antigen receptor (CAR)-T-cell therapy in non-small-cell lung cancer*
1038 *(NSCLC): current status and future perspectives*. Cancer Immunology, Immunotherapy,
1039 2021. **70**(3): p. 619-631.
1040 34. Zhang, Y., et al., *Phase I clinical trial of EGFR-specific CAR-T cells generated by the*
1041 *piggyBac transposon system in advanced relapsed/refractory non-small cell lung cancer*
1042 *patients*. J Cancer Res Clin Oncol, 2021. **147**(12): p. 3725-3734.
1043 35. Giuffrida, L., et al., *CRISPR/Cas9 mediated deletion of the adenosine A2A receptor*
1044 *enhances CAR T cell efficacy*. Nature Communications, 2021. **12**(1).
1045 36. Líndez, A.-A.M., et al., *Mitochondrial arginase-2 is a cell-autonomous regulator of CD8+ T*
1046 *cell function and antitumor efficacy*. JCI Insight, 2019. **4**(24).
1047 37. Kumar, J., et al., *Deletion of Cbl-b inhibits CD8 T-cell exhaustion and promotes CAR T-cell*
1048 *function*. Journal for ImmunoTherapy of Cancer, 2021. **9**(1): p. e001688.
1049 38. Alotaibi, F., et al., *CD5 blockade enhances ex vivo CD8+ T cell activation and tumour cell*
1050 *cytotoxicity*. European Journal of Immunology, 2020. **50**(5): p. 695-704.
1051 39. Shi, L., et al., *CRISPR knock out CTLA-4 enhances the anti-tumor activity of cytotoxic T*
1052 *lymphocytes*. Gene, 2017. **636**: p. 36-41.
1053 40. Pedicord, V.A., et al., *Single dose of anti–CTLA-4 enhances CD8 + T-cell memory*
1054 *formation, function, and maintenance*. Proceedings of the National Academy of Sciences,
1055 2011. **108**(1): p. 266-271.
1056 41. Riese, M.J., et al., *Enhanced Effector Responses in Activated CD8+ T Cells Deficient in*
1057 *Diacylglycerol Kinases*. Cancer Research, 2013. **73**(12): p. 3566-3577.
1058 42. Yamamoto, T.N., et al., *T cells genetically engineered to overcome death signaling*
1059 *enhance adoptive cancer immunotherapy*. Journal of Clinical Investigation, 2019. **129**(4):
1060 p. 1551-1565.
1061 43. Ren, J., et al., *A versatile system for rapid multiplex genome-edited CAR T cell generation*.
1062 Oncotarget, 2017. **8**(10): p. 17002-17011.

44. Si, J., et al., *Hematopoietic Progenitor Kinase1 (HPK1) Mediates T Cell Dysfunction and Is a Druggable Target for T Cell-Based Immunotherapies*. Cancer Cell, 2020. **38**(4): p. 551-566 e11.
45. Good, C.R., et al., *An NK-like CAR T cell transition in CAR T cell dysfunction*. Cell, 2021. **184**(25): p. 6081-6100.e26.
46. Shang, K., et al., *Gene silencing of indoleamine 2,3-dioxygenase 1 inhibits lung cancer growth by suppressing T-cell exhaustion*. Oncology Letters, 2020.
47. Senz, A., et al. *P06.05 IDO1-deleted CAR T cells show improved therapeutic efficacy in murine pancreatic cancer models*. BMJ Publishing Group Ltd.
48. Wang, D., et al., *CRISPR Screening of CAR T Cells and Cancer Stem Cells Reveals Critical Dependencies for Cell-Based Therapies*. Cancer Discovery, 2021. **11**(5): p. 1192-1211.
49. Lukhele, S., et al., *The transcription factor IRF2 drives interferon-mediated CD8(+) T cell exhaustion to restrict anti-tumor immunity*. Immunity, 2022. **55**(12): p. 2369-2385 e10.
50. Liu, X., et al., *Genome-wide analysis identifies NR4A1 as a key mediator of T cell dysfunction*. Nature, 2019. **567**(7749): p. 525-529.
51. Chen, J., et al., *NR4A transcription factors limit CAR T cell function in solid tumours*. Nature, 2019. **567**(7749): p. 530-534.
52. Jung, I.Y., et al., *BLIMP1 and NR4A3 transcription factors reciprocally regulate antitumor CAR T cell stemness and exhaustion*. Sci Transl Med, 2022. **14**(670): p. eabn7336.
53. Janelle, V., et al., *p16(INK4a) Regulates Cellular Senescence in PD-1-Expressing Human T Cells*. Front Immunol, 2021. **12**: p. 698565.
54. Gurusamy, D., et al., *Multi-phenotype CRISPR-Cas9 Screen Identifies p38 Kinase as a Target for Adoptive Immunotherapies*. Cancer Cell, 2020. **37**(6): p. 818-833 e9.
55. Ye, L., et al., *In vivo CRISPR screening in CD8 T cells with AAV–Sleeping Beauty hybrid vectors identifies membrane targets for improving immunotherapy for glioblastoma*. Nature Biotechnology, 2019. **37**(11): p. 1302-1313.
56. Yoshikawa, T., et al., *Genetic ablation of PRDM1 in antitumor T cells enhances therapeutic efficacy of adoptive immunotherapy*. Blood, 2022. **139**(14): p. 2156-2172.
57. Wiede, F., et al., *PTP1B Is an Intracellular Checkpoint that Limits T-cell and CAR T-cell Antitumor Immunity*. Cancer Discov, 2022. **12**(3): p. 752-773.
58. Wiede, F., et al., *PTPN2 phosphatase deletion in T cells promotes anti-tumour immunity and CAR T-cell efficacy in solid tumours*. The EMBO Journal, 2020. **39**(2).
59. Carnevale, J., et al., *RASA2 ablation in T cells boosts antigen sensitivity and long-term function*. Nature, 2022. **609**(7925): p. 174-182.
60. Weisshaar, N., et al., *Rgs16 promotes antitumor CD8(+) T cell exhaustion*. Sci Immunol, 2022. **7**(71): p. eabh1873.
61. Olesch, C., et al., *S1PR4 ablation reduces tumor growth and improves chemotherapy via CD8+ T cell expansion*. J Clin Invest, 2020. **130**(10): p. 5461-5476.
62. Trefny, M.P., et al., *Deletion of SNX9 alleviates CD8 T cell exhaustion for effective cellular cancer immunotherapy*. Nat Commun, 2023. **14**(1): p. 86.
63. Jain, N., et al., *SUV39H1 disruption imparts functional persistence to CD28-costimulated human CAR T cells*. The Journal of Immunology, 2022. **208**(Supplement_1): p. 122.05-122.05.
64. Lopez-Cobo, S., et al., *SUV39H1 Ablation Enhances Long-term CAR T Function in Solid Tumors*. Cancer Discov, 2024. **14**(1): p. 120-141.
65. Tang, N., et al., *TGF-β inhibition via CRISPR promotes the long-term efficacy of CAR T cells against solid tumors*. JCI Insight, 2020. **5**(4).
66. Jackson, Z., et al., *Sequential Single-Cell Transcriptional and Protein Marker Profiling Reveals TIGIT as a Marker of CD19 CAR-T Cell Dysfunction in Patients with Non-Hodgkin Lymphoma*. Cancer Discov, 2022. **12**(8): p. 1886-1903.

67. Seo, H., et al., *TOX and TOX2 transcription factors cooperate with NR4A transcription factors to impose CD8+ T cell exhaustion*. Proceedings of the National Academy of Sciences, 2019. **116**(25): p. 12410-12415.

68. Song, M., et al., *IRE1α–XBP1 controls T cell function in ovarian cancer by regulating mitochondrial activity*. Nature, 2018. **562**(7727): p. 423-428.
69. Mai, D., et al., *Combined disruption of T cell inflammatory regulators Regnase-1 and Roquin-1 enhances antitumor activity of engineered human T cells*. Proceedings of the National Academy of Sciences, 2023. **120**(12).
70. Gargett, T. and M.P. Brown, *The inducible caspase-9 suicide gene system as a â€œsafety switchâ€ to limit on-target, off-tumor toxicities of chimeric antigen receptor T cells*. Frontiers in Pharmacology, 2014. **5**.
71. Salter, A.I., et al., *Comparative analysis of TCR and CAR signaling informs CAR designs with superior antigen sensitivity and in vivo function*. Sci Signal, 2021. **14**(697).
72. Wu, L., et al., *Signaling from T cell receptors (TCRs) and chimeric antigen receptors (CARs) on T cells*. Cell Mol Immunol, 2020. **17**(6): p. 600-612.
73. Zhao, Z., et al., *Structural Design of Engineered Costimulation Determines Tumor Rejection Kinetics and Persistence of CAR T Cells*. Cancer Cell, 2015. **28**(4): p. 415-428.
74. Cappell, K.M. and J.N. Kochenderfer, *A comparison of chimeric antigen receptors containing CD28 versus 4-1BB costimulatory domains*. Nat Rev Clin Oncol, 2021. **18**(11): p. 715-727.
75. Philipson, B.I., et al., *4-1BB costimulation promotes CAR T cell survival through noncanonical NF-kappaB signaling*. Sci Signal, 2020. **13**(625).
76. Simula, L., et al., *Mitochondrial metabolism sustains CD8(+) T cell migration for an efficient infiltration into solid tumors*. Nat Commun, 2024. **15**(1): p. 2203.
77. Kallies, A., D. Zehn, and D.T. Utzschneider, *Precursor exhausted T cells: key to successful immunotherapy?* Nat Rev Immunol, 2020. **20**(2): p. 128-136.
78. Zheng, W., et al., *Regnase-1 suppresses TCF-1+ precursor exhausted T-cell formation to limit CAR–T-cell responses against ALL*. Blood, 2021. **138**(2): p. 122-135.
79. Si, X., et al., *Preclinical Evaluation of CAR T Cell Function: In Vitro and In Vivo Models*. International Journal of Molecular Sciences, 2022. **23**(6): p. 3154.
80. Arunachalam, A.K., et al., *Advancing CAR T-cell therapies: Preclinical insights and clinical translation for hematological malignancies*. Blood Rev, 2024. **68**: p. 101241.
81. Stribbling, S.M., C. Beach, and A.J. Ryan, *Orthotopic and metastatic tumour models in preclinical cancer research*. Pharmacol Ther, 2024. **257**: p. 108631.
82. Melssen, M.M., et al., *Barriers to immune cell infiltration in tumors*. Journal for ImmunoTherapy of Cancer, 2023. **11**(4): p. e006401.
83. Donnadieu, E., et al., *Surmounting the obstacles that impede effective CAR T cell trafficking to solid tumors*. Journal of Leukocyte Biology, 2020. **108**(4): p. 1067-1079.
84. Katz, S.C., et al., *Phase I Hepatic Immunotherapy for Metastases Study of Intra-Arterial Chimeric Antigen Receptor–Modified T-cell Therapy for CEA+ Liver Metastases*. Clinical Cancer Research, 2015. **21**(14): p. 3149-3159.
85. Zhao, Y., et al., *IL-10-expressing CAR T cells resist dysfunction and mediate durable clearance of solid tumors and metastases*. Nat Biotechnol, 2024. **42**(11): p. 1693-1704.
86. Hou, A.J., L.C. Chen, and Y.Y. Chen, *Navigating CAR-T cells through the solid-tumour microenvironment*. Nat Rev Drug Discov, 2021. **20**(7): p. 531-550.
87. Schurich, A., I. Magalhaes, and J. Mattsson, *Metabolic regulation of CAR T cell function by the hypoxic microenvironment in solid tumors*. Immunotherapy, 2019. **11**(4): p. 335-345.
88. Andreu-Saumell, I., et al., *CAR affinity modulates the sensitivity of CAR-T cells to PD-1/PD-L1-mediated inhibition*. Nature Communications, 2024. **15**(1).
89. Korell, F., et al., *In vivo CRISPR screens identify key modifiers of CAR T cell function in myeloma*. bioRxiv preprint, 2024.

90. Bloh, K., et al., *Deconvolution of Complex DNA Repair (DECODR): Establishing a Novel Deconvolution Algorithm for Comprehensive Analysis of CRISPR-Edited Sanger Sequencing Data*. The CRISPR Journal, 2021. **4**(1): p. 120-131.
91. Cash, W., *Parameter estimation in astronomy through application of the likelihood ratio*. The Astrophysical Journal, 1979. **228**: p. 939.
92. Simoni, Y., et al., *Bystander CD8(+) T cells are abundant and phenotypically distinct in human tumour infiltrates*. Nature, 2018. **557**(7706): p. 575-579.
93. Simoni, Y., et al., *Human Innate Lymphoid Cell Subsets Possess Tissue-Type Based Heterogeneity in Phenotype and Frequency*. Immunity, 2018. **48**(5): p. 1060.
94. Li, S., et al., *Bystander CD4 + T cells infiltrate human tumors and are phenotypically distinct*. OncoImmunology, 2022. **11**(1).
95. Moore, W.A. and D.R. Parks, *Update for the logicle data scale including operational code implementations*. Cytometry Part A, 2012. **81A**(4): p. 273-277.

Figure 1

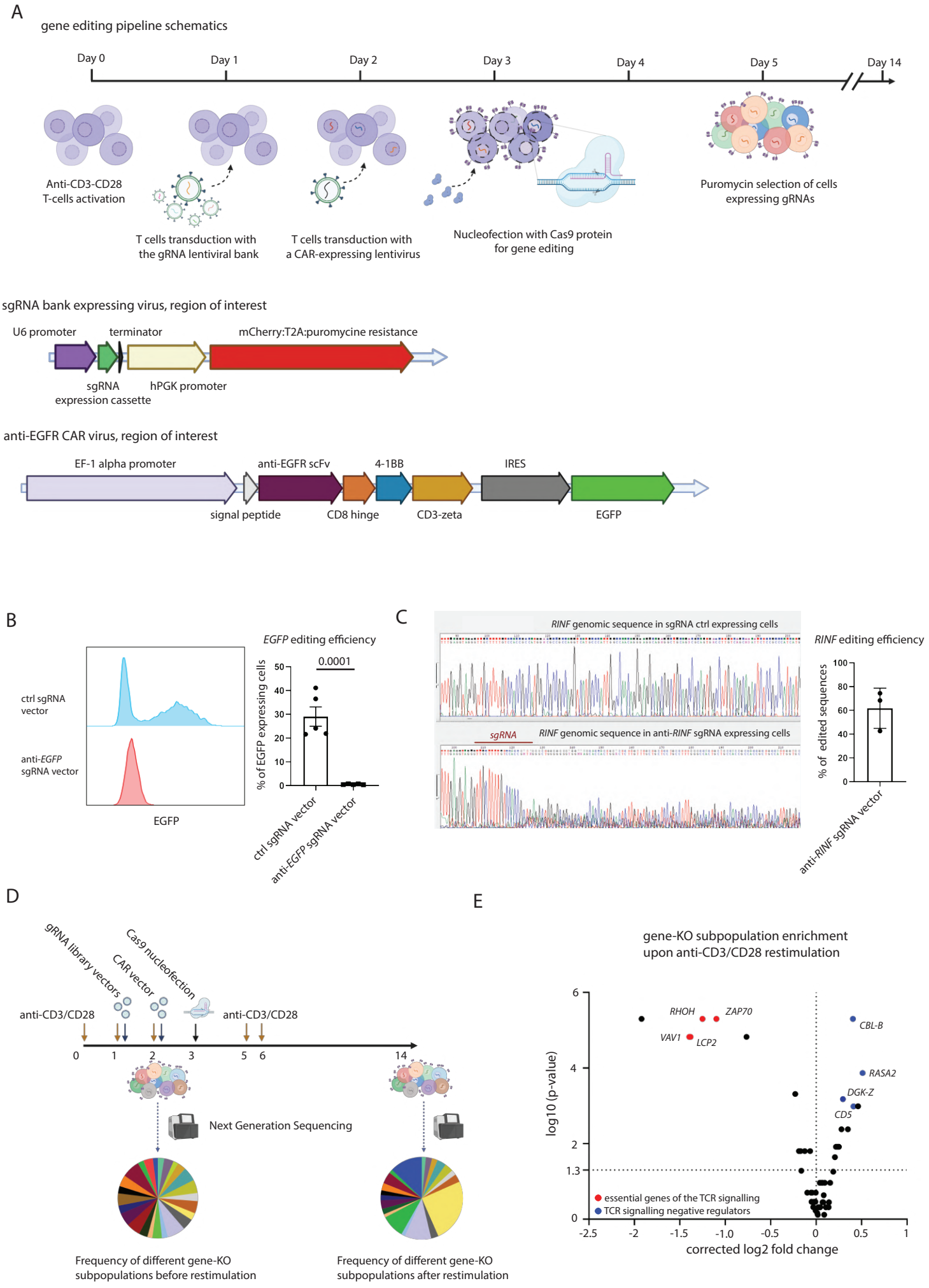
A
gene editing pipeline schematics
Day 0
Day 1
Day 2
Day 3
Day 4
Day 5
Day 14
Anti-CD3-CD28
T-cells activation
T cells transduction with
the gRNA lentiviral bank
T cells transduction with
a CAR-expressing lentivirus
Nucleofection with Cas9 protein
for gene editing
Puromycin selection of cells
expressing gRNAs
sgRNA bank expressing virus, region of interest
U6 promoter
terminator
mCherry:T2A:puromycine resistance
sgRNA
expression cassette
hPGK promoter
anti-EGFR CAR virus, region of interest
EF-1 alpha promoter
anti-EGFR scFv
4-1BB
IRES
signal peptide
CD8 hinge
CD3-zeta
EGFP
B
ctrl sgRNA
vector
anti-EGFP
sgRNA vector
EGFP
EGFP editing efficiency
0.0001
% of EGFP expressing cells
50
40
30
20
10
0
ctrl sgRNA vector
anti-EGFP sgRNA vector
C
RINF genomic sequence in sgRNA ctrl expressing cells
sgRNA
RINF genomic sequence in anti-RINF sgRNA expressing cells
RINF editing efficiency
% of edited sequences
100
80
60
40
20
0
anti-RINF sgRNA vector
D
gRNA library vectors
CAR vector
Cas9 nucleofection
anti-CD3/CD28
anti-CD3/CD28
0
1
2
3
5
6
14
Next Generation Sequencing
Frequency of different gene-KO
subpopulations before restimulation
Frequency of different gene-KO
subpopulations after restimulation
E
gene-KO subpopulation enrichment
upon anti-CD3/CD28 restimulation
log10 (p-value)
6
4
2
1.3
0
RHOH
ZAP70
VAV1
LCP2
CBL-B
RASA2
DGK-Z
CD5
essential genes of the TCR signalling
TCR signalling negative regulators
-2.5
-2
-1.5
-1.0
-0.5
0
0.5
1
corrected log2 fold change

Figure 1: **(A)** CAR-T cells editing strategy schematics. **(B)** Validation of gene editing strategy by a pilot system targeting *EGFP* in EGFP expressing T cells, as evaluated by signal loss upon knock out trough flow cytometry. p-value of unpaired t-test. **(C)** Validation of gene editing strategy by a pilot system targeting the gene *RINF* in T cells, as evaluated by proportion of modified genomic sequences upon knock out, determined through sanger sequencing and deconvolution analysis of chromatograms files. **(D)** Validation of the overall pipeline and of lentiviral bank efficacy by assessing frequency reduction of cells expressing gRNAs targeting genes essential for TCR signalling, used as negative control genes. log2 fold change for each gene, expressing frequency changes between the two time points, is corrected to average log2 fold change for 20 non-targeting gRNA.

Figure 2

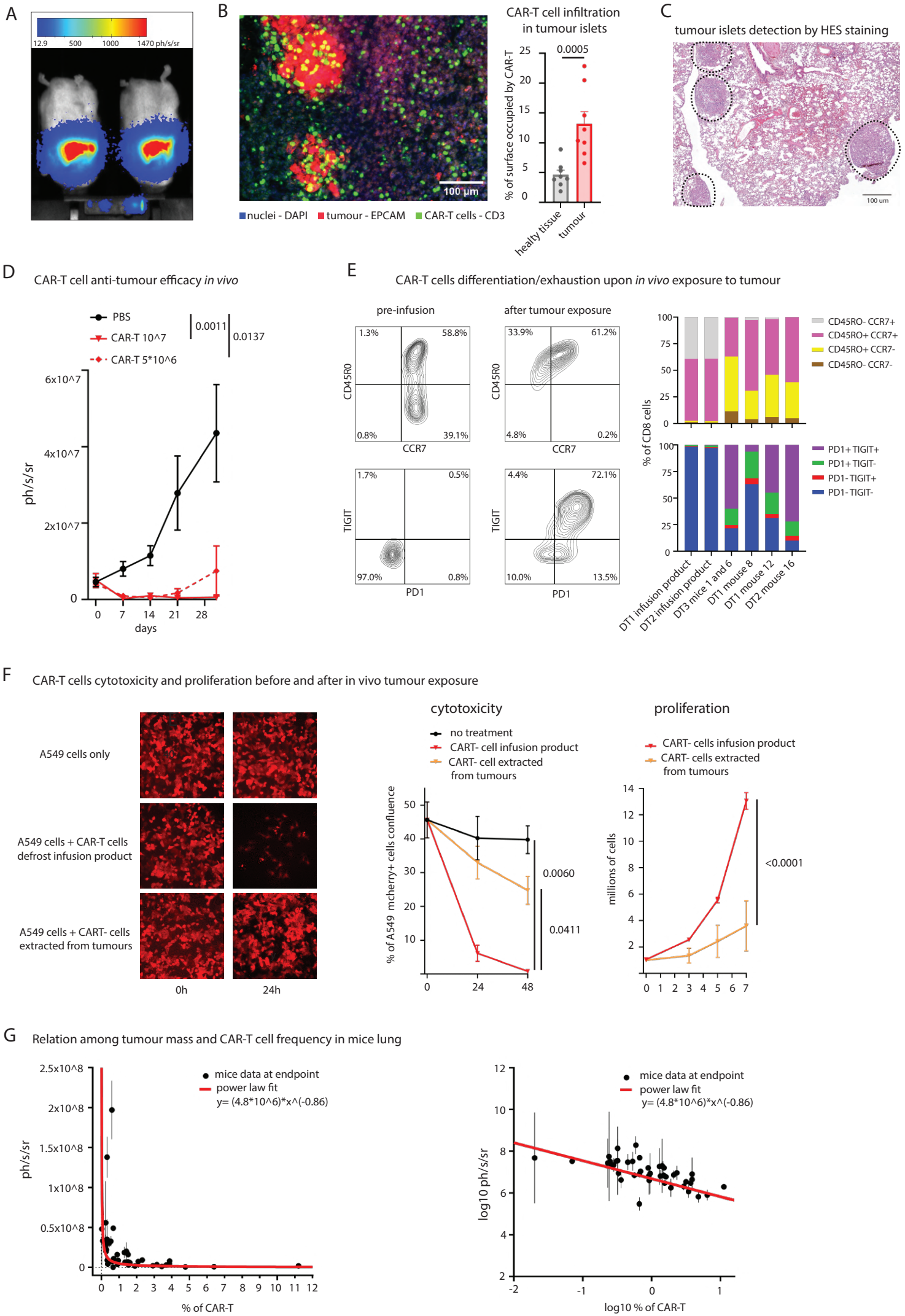
A
12.9
500
1000
1470 ph/s/sr
B
100 µm
nuclei - DAPI
tumour - EPCAM
CAR-T cells - CD3
CAR-T cell infiltration in tumour islets
0.0005
% of surface occupied by CAR-T
healty tissue
tumour
C
tumour islets detection by HES staining
100 um
D
CAR-T cell anti-tumour efficacy in vivo
PBS
CAR-T 10^7
CAR-T 5*10^6
0.0011
0.0137
ph/s/sr
days
E
CAR-T cells differentiation/exhaustion upon in vivo exposure to tumour
pre-infusion
after tumour exposure
CD45RO
CCR7
TIGIT
PD1
1.3%
58.8%
0.8%
39.1%
33.9%
61.2%
4.8%
0.2%
1.7%
0.5%
97.0%
0.8%
4.4%
72.1%
10.0%
13.5%
% of CD8 cells
CD45RO- CCR7+
CD45RO+ CCR7+
CD45RO+ CCR7-
CD45RO- CCR7-
PD1+ TIGIT+
PD1+ TIGIT-
PD1- TIGIT+
PD1- TIGIT-
DT1 infusion product
DT2 infusion product
DT3 mice 1 and 6
DT1 mouse 8
DT1 mouse 12
DT2 mouse 16
F
CAR-T cells cytotoxicity and proliferation before and after in vivo tumour exposure
A549 cells only
A549 cells + CAR-T cells defrost infusion product
A549 cells + CART- cells extracted from tumours
0h
24h
cytotoxicity
no treatment
CART- cell infusion product
CART- cell extracted from tumours
% of A549 mcherry+ cells confluence
0.0060
0.0411
proliferation
CART- cells infusion product
CART- cells extracted from tumours
millions of cells
<0.0001
G
Relation among tumour mass and CAR-T cell frequency in mice lung
mice data at endpoint
power law fit
y= (4.8*10^6)*x^(-0.86)
ph/s/sr
% of CAR-T
log10 ph/s/sr
log10 % of CAR-T

Figure 2: **(A)** Bioluminescence live imaging of A549 cells orthotopic lung tumour. **(B)** Immunofluorescence microscopy image of A549 cells (EpCAM staining in red) tumour islet in mice lung, with CAR-T infiltrate (human CD3 staining cells in green). Infiltration analysis has been performed on tumour bearing lung slices images (n=8). p-values are calculated by one-way ANOVA test. **(C)** Haematoxylin Eosin staining of lung tumour section. **(D)** Tumour growth curve, assessed by bioluminescence analysis, in mice receiving mock solution (n=5) or treated with 10^7 CAR-T cells(n=3) or 5*10^6 CAR-T cells(n=5). p-values are calculated by two-ways ANOVA test, results for whole curves comparisons are shown. **(E)** Phenotypical characterisation of CAR-T cells by flow cytometry. We compared CAR-T cells from infusion products and CAR-T cells recovered from mice which received the 5*10^6 dose after long term exposure to tumour *in vivo*. **(F)** Functional characterisation CAR-T cells from infusion products and CAR-T cells recovered from mice. Cytotoxic capacity was assessed by calculating surface reduction of mCherry+ tumour cells when co-cultured with CAR-T cells.(at least 3 images were taken per condition, at each time point) Proliferation capacity was assessed by cell counting upon 7 days after anti-CD3/C28 stimulation. (n=3 biological replicates for pre-infusion CAR-T cells, n=4 for mice extracted CAR-T cells) p-values are calculated by two-ways ANOVA test, results for final time point comparisons are shown. **(G)** (left) Power-law defined negative correlation among tumour mass, assessed by bioluminescence, and % of CAR-T cells in mice lung at the experiment endpoint. Data shown are collected from all screening experiments performed. The represented power law has been defined through data fitting. (right) representation of the same data and fitting curve on log10 axes.

Figure 3

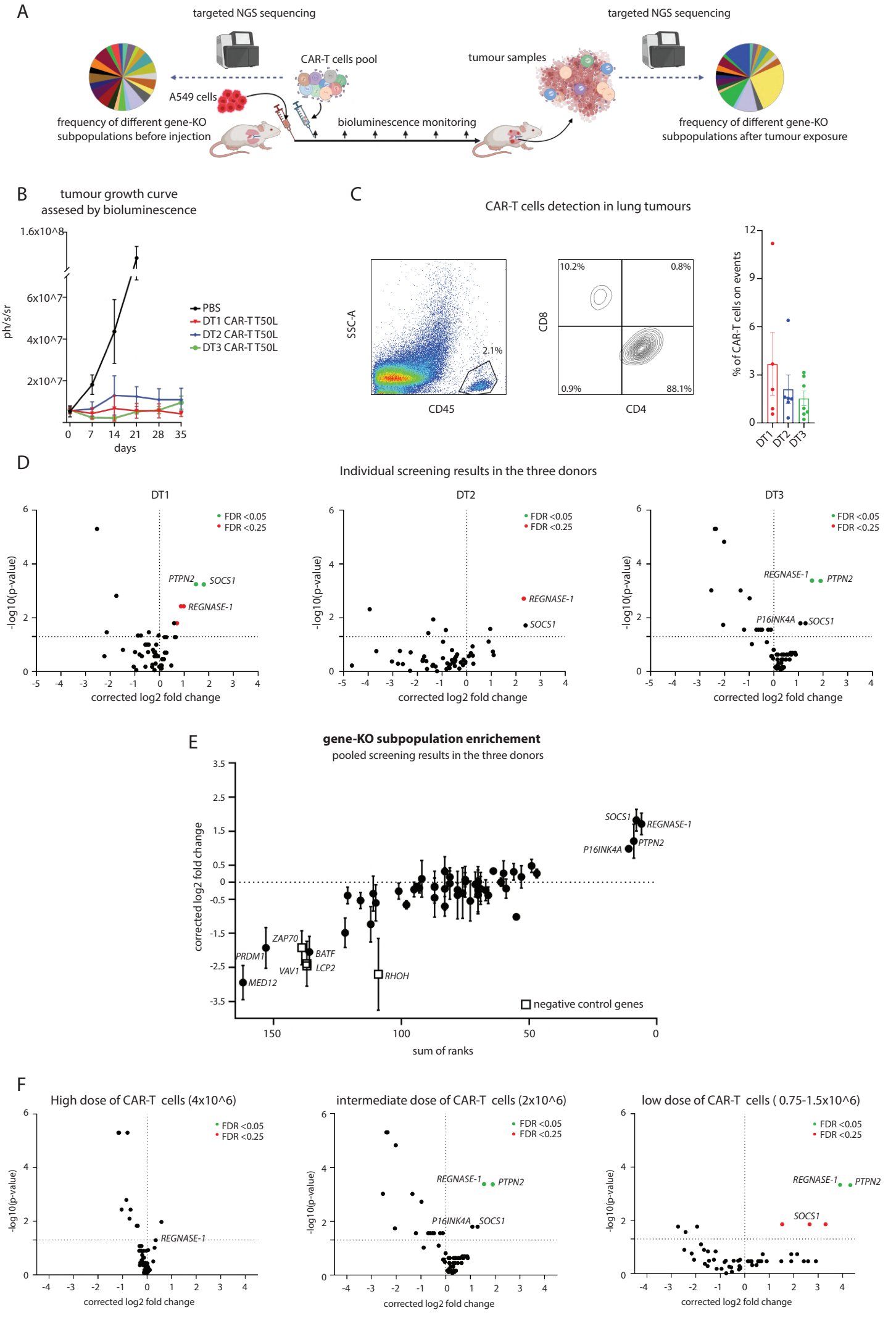
A
targeted NGS sequencing
CAR-T cells pool
A549 cells
frequency of different gene-KO subpopulations before injection
bioluminescence monitoring
tumour samples
targeted NGS sequencing
frequency of different gene-KO subpopulations after tumour exposure
B
tumour growth curve assesed by bioluminescence
ph/s/sr
1.6x10^8
6x10^7
4x10^7
2x10^7
PBS
DT1 CAR-T T50L
DT2 CAR-T T50L
DT3 CAR-T T50L
days
C
CAR-T cells detection in lung tumours
SSC-A
CD45
2.1%
CD8
CD4
10.2%
0.8%
0.9%
88.1%
% of CAR-T cells on events
DT1
DT2
DT3
D
Individual screening results in the three donors
DT1
DT2
DT3
FDR <0.05
FDR <0.25
-log10(p-value)
corrected log2 fold change
PTPN2
SOCS1
REGNASE-1
P16INK4A
E
gene-KO subpopulation enrichement
pooled screening results in the three donors
corrected log2 fold change
sum of ranks
SOCS1
REGNASE-1
PTPN2
P16INK4A
ZAP70
PRDM1
BATF
VAV1
LCP2
MED12
RHOH
negative control genes
F
High dose of CAR-T cells (4x10^6)
intermediate dose of CAR-T cells (2x10^6)
low dose of CAR-T cells (0.75-1.5x10^6)
FDR <0.05
FDR <0.25
-log10(p-value)
corrected log2 fold change
REGNASE-1
PTPN2
P16INK4A
SOCS1

Figure 3: **(A)** Schematics of the experiment. **(B)** Tumour growth curve as determined by bioluminescence for mice treated either with excipient (n=5) or 2*10^6 CAR-T modified with our T50L (Top 50 library) lentivirus bank, from three different donors DT1 (n=5), DT2 (n=6), DT3 (n=7) (C) CAR-T cells detection in mice lungs by flow cytometry. **(D)** Screening results for CAR-T cells from the three different donors, gene-ko subpopulation proportions are compared in mice lungs at the endpoint of the experiment vs in infusion products. log2 fold change for each gene, expressing frequency changements between the two time points, is corrected to average log2 fold change for 20 non-targeting gRNA. p-values are determined by MAGeCK permutation test and FDR values are calculated with Benjamini-Hochberg correction. **(E)** Overall results pooling the three independent screenings, log2 fold change for each gene is calculated as average of these values from each individual screenings. Sum of rank value is determined as sum of the rankings assigned by MAGeCK alpha-RRA algorithm for each gene in the three screenings. **(F)** Screening results from three different experiments in which either 4*10^6 CAR-T T50L, 2*10^6 CAR-T T50L or 0.75-1.5*10^6 CAR-T T50L were injected to mice, with progressively less effective tumour control, and therefore increasing selective pressure on CAR-T cells. gene-ko subpopulation proportions are compared in mice lungs at the endpoint of the experiment vs in infusion products. log2 fold change for each gene, expressing frequency changes between the two time points, is corrected to average log2 fold change for 20 non-targeting gRNA. p-values are determined by MAGeCK permutation test and FDR values are calculated with Benjamini-Hochberg correction.

Figure 4

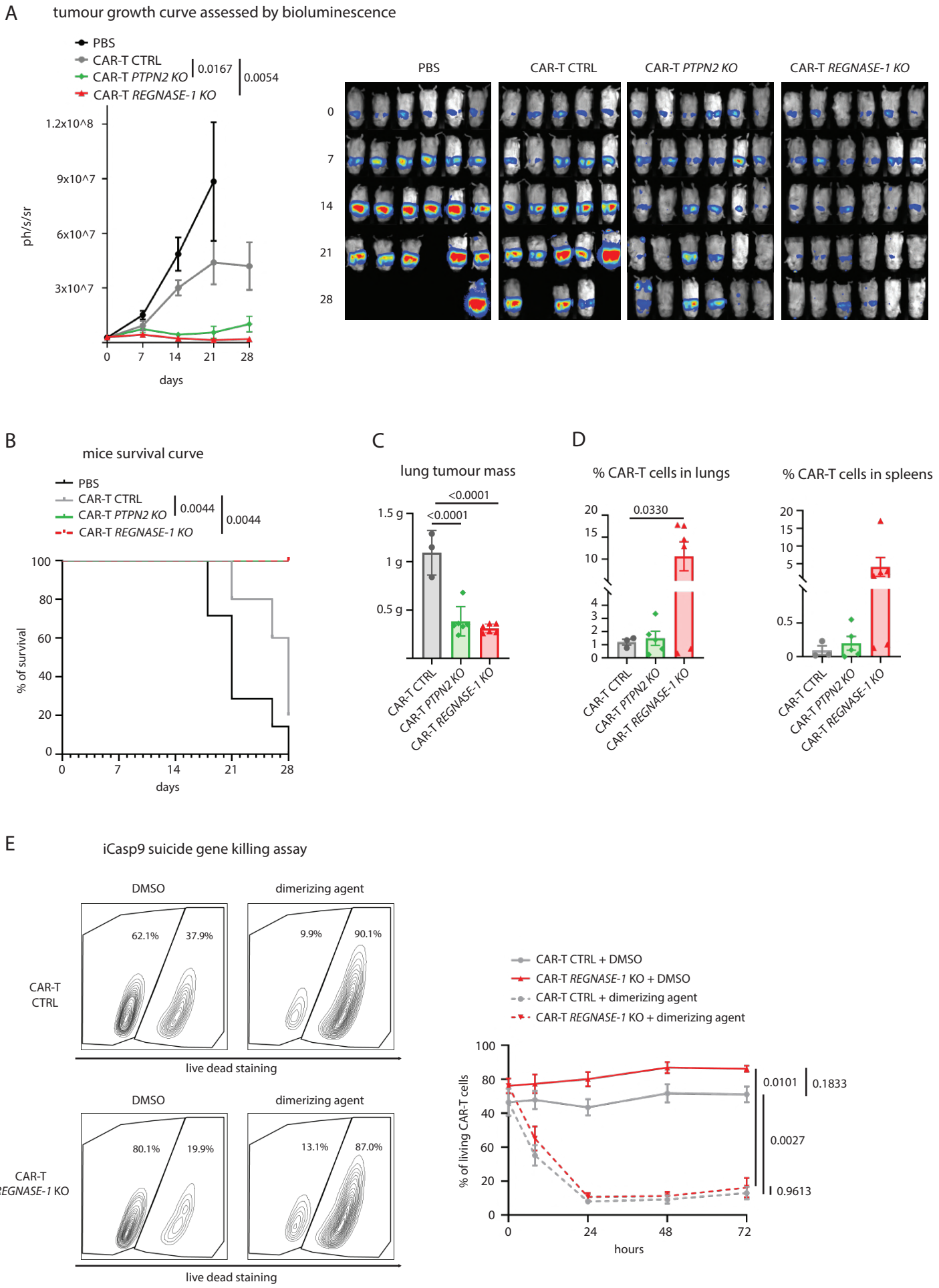
A
tumour growth curve assessed by bioluminescence
PBS
CAR-T CTRL
CAR-T PTPN2 KO
CAR-T REGNASE-1 KO
0.0167
0.0054
1.2x10^8
9x10^7
6x10^7
3x10^7
ph/s/sr
0
7
14
21
28
days
PBS
CAR-T CTRL
CAR-T PTPN2 KO
CAR-T REGNASE-1 KO
B
mice survival curve
PBS
CAR-T CTRL
CAR-T PTPN2 KO
CAR-T REGNASE-1 KO
0.0044
0.0044
100
80
60
40
20
0
% of survival
days
C
lung tumour mass
<0.0001
<0.0001
1.5 g
1 g
0.5 g
CAR-T CTRL
CAR-T PTPN2 KO
CAR-T REGNASE-1 KO
D
% CAR-T cells in lungs
0.0330
% CAR-T cells in spleens
E
iCasp9 suicide gene killing assay
DMSO
dimerizing agent
CAR-T CTRL
62.1%
37.9%
9.9%
90.1%
live dead staining
CAR-T REGNASE-1 KO
80.1%
19.9%
13.1%
87.0%
CAR-T CTRL + DMSO
CAR-T REGNASE-1 KO + DMSO
CAR-T CTRL + dimerizing agent
CAR-T REGNASE-1 KO + dimerizing agent
% of living CAR-T cells
hours
0.0101
0.1833
0.0027
0.9613

Figure 4: **(A)** Tumour growth curve in mice treated either with excipient (n=6), 10^6 CTRL CAR-T cells (n=5), 10^6 *PTPN2* KO CAR-T cells (n=6) or 10^6 *REGNASE-1* KO CAR-T cells (n=6). p-values are calculated by two-ways ANOVA test, results for whole curves comparisons are shown. Individual images for each mouse at different time points on the right. **(B)** Survival curves for mice treated with the aforementioned conditions. P-values have been determined by log-rank mantel-cox test. **(C)** Lung size at endpoint, indicative of tumour mass, p-values are calculated by one-way ANOVA test. **(D)** % of CAR-T cells in lungs and spleens of mice at the endpoint as determined by flow cytometry. **(E)** CAR-T cells killing by the safety switch system iCasp9 gene, upon administration of dimerizing agent. Unmodified CAR-T cells (n=3) are compared to *REGNASE-1* KO CAR-T cells (n=3). Cell death was determined by flow cytometry analysis with live-dead blue dye, data are corrected to cells numbers, to account for dead cell lysis. p-values are calculated by two-ways ANOVA test, results for final time point are shown.

Figure 5

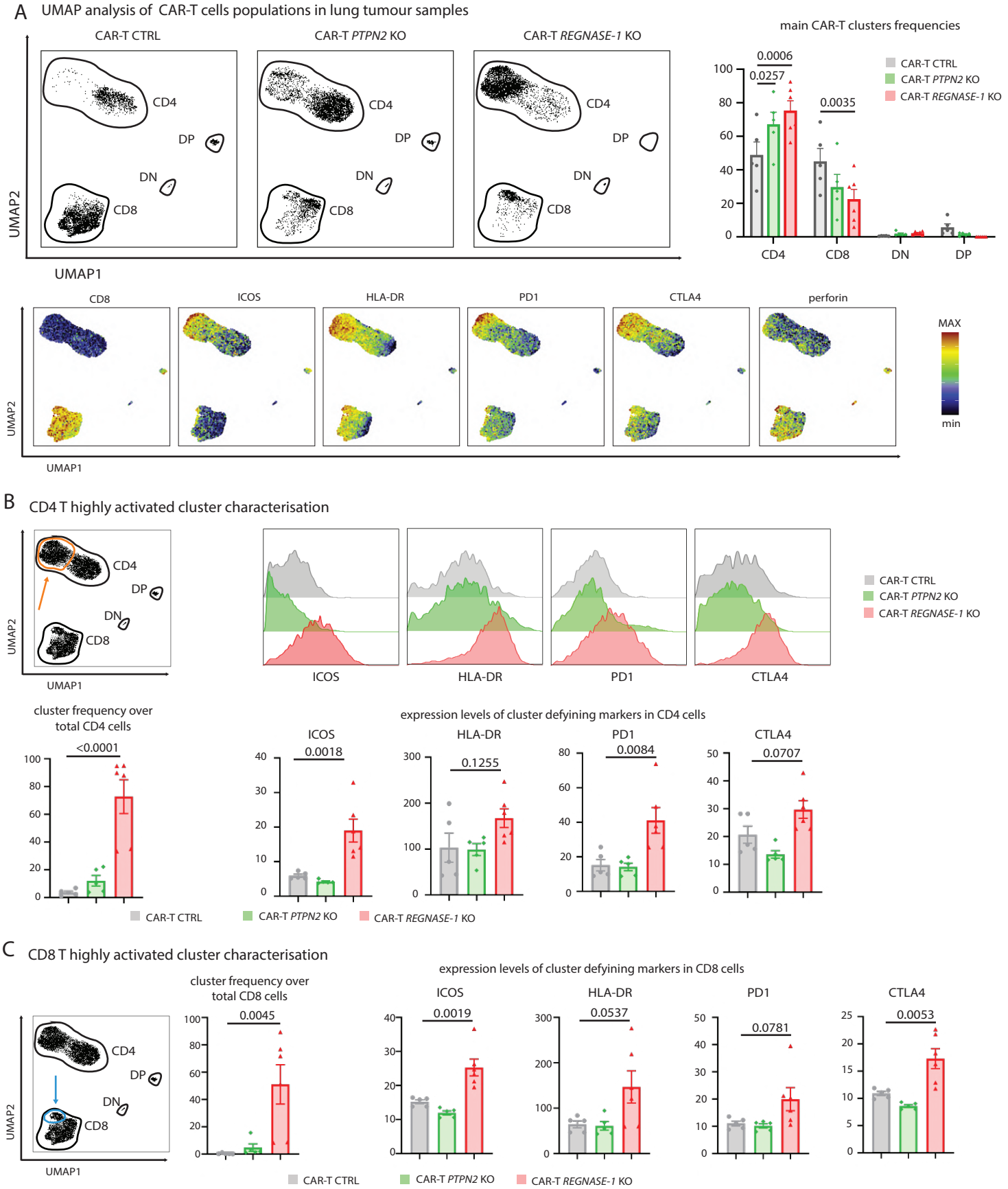
A
UMAP analysis of CAR-T cells populations in lung tumour samples
CAR-T CTRL
CAR-T PTPN2 KO
CAR-T REGNASE-1 KO
CD4
DP
DN
CD8
UMAP2
UMAP1
main CAR-T clusters frequencies
0.0006
0.0257
0.0035
CAR-T CTRL
CAR-T PTPN2 KO
CAR-T REGNASE-1 KO
CD8
ICOS
HLA-DR
PD1
CTLA4
perforin
MAX
min
B
CD4 T highly activated cluster characterisation
ICOS
HLA-DR
PD1
CTLA4
cluster frequency over total CD4 cells
<0.0001
expression levels of cluster defying markers in CD4 cells
0.0018
0.1255
0.0084
0.0707
C
CD8 T highly activated cluster characterisation
cluster frequency over total CD8 cells
0.0045
expression levels of cluster defying markers in CD8 cells
0.0019
0.0537
0.0781
0.0053
D
Clustered heatmap representation of all markers expression in different subsets
double positive cluster
CD4 highly activated cluster
CD4 CTRL cluster
CD8 highly activated cluster
CD8 CTRL cluster
Double negative cluster
CD3
CD29
HLA-DR
CD8
GranzymeA
GranzymeB
CD69
CD45RO
CTLA-4
PD-1
CD4
CXCR4
CD38
CCR7
ICOS
CD28
Perforin
GranzymeK
CD56
Granulysin
2B4
KLRG1
CD103
TIGIT
CD226
CD39
CD36
CD25
CD127
CD20
OX40
CD57

Figure 5: **(A)** UMAP analysis of Cytometry by Time of Flight (CyToF) data from CAR-T cells in lung tumour samples at the endpoint of the experiment. Relative proportion of main clusters (upper right) and main markers of interests (bottom) in samples from CTRL (n=5), *REGNASE-1* KO (n=6) and *PTPN2* KO (n=5) are also shown. p-values are calculated by one-way ANOVA test. **(B)** Characterisation of variations within the CD4 cluster. the formation of a sub-cluster, for the *REGNASE-1* KO condition, is shown in the combinatory graph of the three exemplary samples (top left) variations of expression for markers defining such cluster in the 3 different exemplary samples are then shown (top right). Frequency of such cluster among all samples and expression levels for the aforementioned markers are shown (respectively bottom left and bottom right) p-values are calculated by one way ANOVA test. **(C)** Characterisation of variations within the CD8 cluster. the formation of a sub-cluster, for the *REGNASE-1* KO condition, is shown in the combinatory graph of the three exemplary samples (left) overall variations of expression for markers defining such cluster in different condition are then shown (top right). Frequency of such cluster among all samples and expression levels for the aforementioned markers are shown (respectively bottom left and bottom right) p-values are calculated by one way ANOVA test. **(D)** Clustered heatmap and relative dendrogram, data are calculated as overall variation of different markers among defined clusters in all samples.

Figure 6

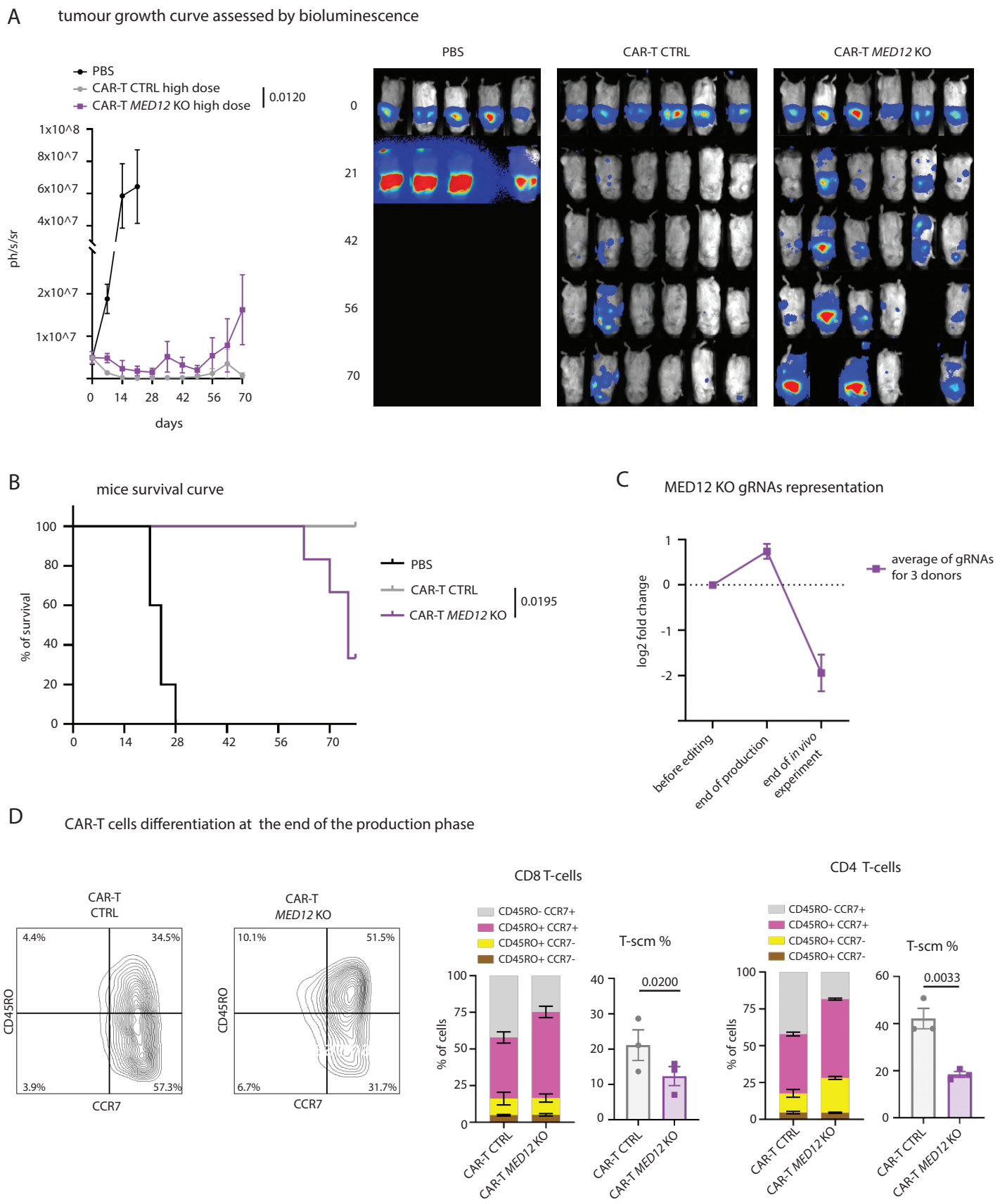
A
tumour growth curve assessed by bioluminescence
PBS
CAR-T CTRL high dose
CAR-T MED12 KO high dose
0.0120
ph/s/sr
days
PBS
CAR-T CTRL
CAR-T MED12 KO
B
mice survival curve
% of survival
PBS
CAR-T CTRL
CAR-T MED12 KO
0.0195
C
MED12 KO gRNAs representation
log2 fold change
average of gRNAs for 3 donors
before editing
end of production
end of in vivo experiment
D
CAR-T cells differentiation at the end of the production phase
CAR-T CTRL
CAR-T MED12 KO
CD45RO
CCR7
4.4%
34.5%
3.9%
57.3%
10.1%
51.5%
6.7%
31.7%
CD8 T-cells
CD4 T-cells
CD45RO- CCR7+
CD45RO+ CCR7+
CD45RO+ CCR7-
CD45RO+ CCR7-
% of cells
T-scm %
0.0200
0.0033

Figure 6: **(A)** Tumour growth curve in mice treated either with excipient (n=5), 3*10^6 CTRL CAR-T cells (n=6) or 3*10^6 *MED12* KO CAR-T cells (n=6). In reason of the great disparity of signal within mice of the same groups p-value are calculated by non-parametric Wilcoxon signed rank test, results for whole curves comparisons are shown. (nonetheless, p-value of 2-way Anova is also significative, p=0.0002) Individual images for each mouse at different time points on the right. **(B)** Survival curves for mice treated with the aforementioned conditions. P-values have been determined by log-rank mantel-cox test. **(C)** Log2 fold change variations in frequencies of gRNAs targeting *MED12*, through different time points. variations are normalised to non-targeting guides and are calculated as average values for all sgRNA in the three donors. **(D)** Flow cytometry based differentiation profiling for *MED12* KO CAR-T cells (n=3) as compared to CTRL CAR-T cells (n=3) at the endpoint of production phase. T-scm (T stem cell memory) are defined as CD45RA+ and CD27+ t-cells. P-values are calculated with paired ratio t-tests.

Figure 7

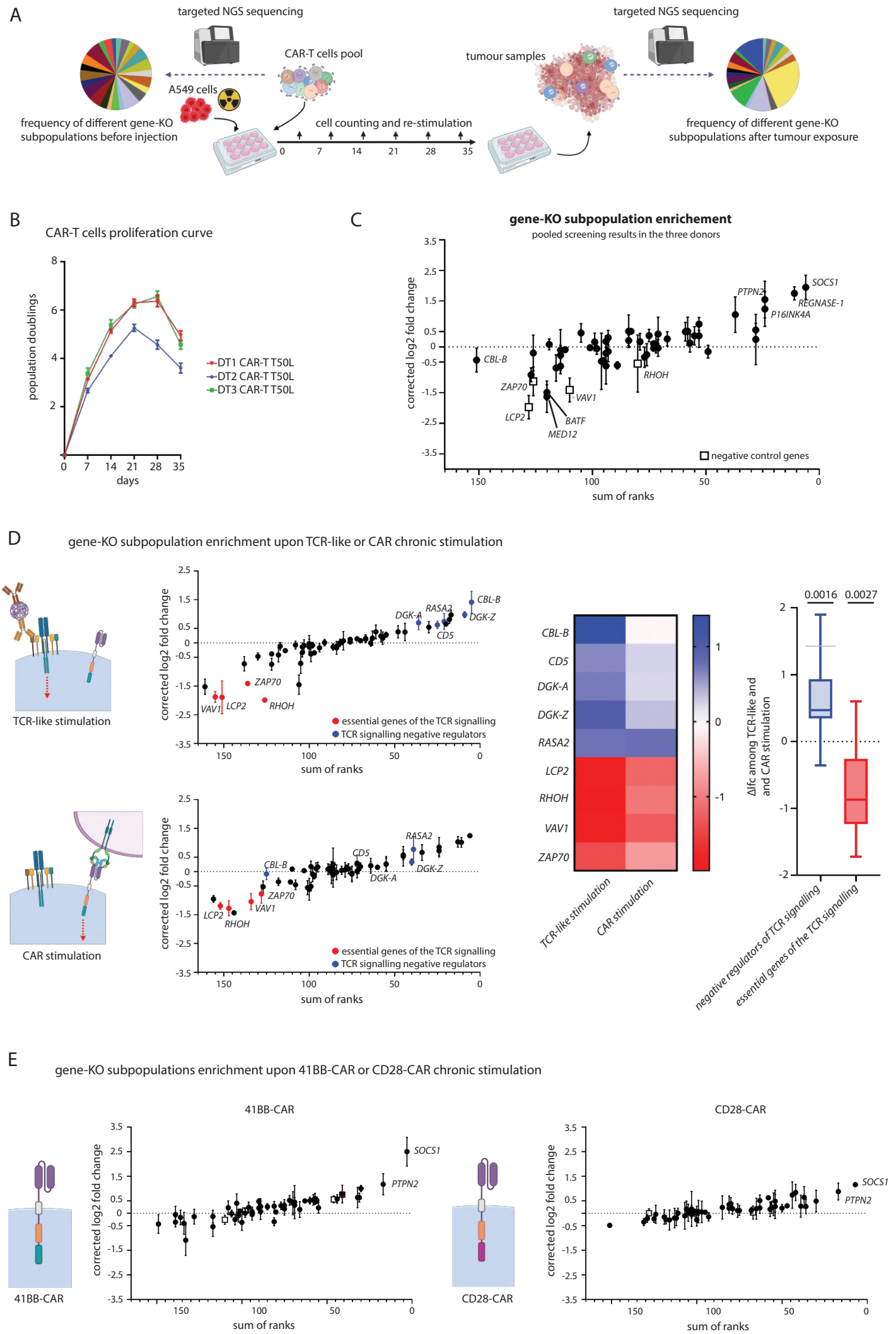
A
targeted NGS sequencing
CAR-T cells pool
A549 cells
frequency of different gene-KO subpopulations before injection
cell counting and re-stimulation
0 7 14 21 28 35
tumour samples
targeted NGS sequencing
frequency of different gene-KO subpopulations after tumour exposure
B
CAR-T cells proliferation curve
population doublings
days
DT1 CAR-T T50L
DT2 CAR-T T50L
DT3 CAR-T T50L
C
gene-KO subpopulation enrichement
pooled screening results in the three donors
corrected log2 fold change
sum of ranks
SOCS1
PTPN2
REGNASE-1
P16INK4A
CBL-B
RHOH
ZAP70
VAV1
LCP2
BATF
MED12
negative control genes
D
gene-KO subpopulation enrichment upon TCR-like or CAR chronic stimulation
TCR-like stimulation
CAR stimulation
essential genes of the TCR signalling
TCR signalling negative regulators
CBL-B
DGK-A
RASA2
DGK-Z
CD5
ZAP70
VAV1
LCP2
RHOH
0.0016
0.0027
ΔIfc among TCR-like and and CAR stimulation
negative regulators of TCR signalling
essential genes of the TCR signalling
E
gene-KO subpopulations enrichment upon 41BB-CAR or CD28-CAR chronic stimulation
41BB-CAR
CD28-CAR
SOCS1
PTPN2

Figure 7: **(A)** Schematics of the experiment **(B)** CAR-T cells proliferation curve as determined by cell counting, 3 replicates for each of 3 donors derived CAR-T cells DT1, DT2, DT3 **(C)** Overall results pooling three independent screenings, log2 fold change for each gene is calculated as average of these values from each individual screening. Sum of rank value is determined as sum of the rankings assigned by MAGeCK alpha-RRA algorithm for each gene in the three screenings. gene-ko subpopulation frequency variations are compared at the endpoint of the experiment, 35 days, vs in starting products. **(D)** (left) Screening results from three different experiments in which CAR-T cells either were stimulated by anti-CD3/CD28 polymers or irradiated tumour cells, every 3 to 5 days for 14 days, to assess mainly proliferation effects. gene-ko subpopulation proportions are compared at the endpoint of the experiment vs in starting products. (middle) Heatmap representation of log2 fold change variation for genes either essential to or negatively regulating the TCR pathway. (right) Overall difference in log2 fold change in frequency of CAR-T cells carrying mutation in negative regulators of the TCR pathway and essential genes of this pathway. Variations in CAR-T cells stimulated with anti-CD3/CD28 polymers compared to variations in CAR stimulated CAR-T cells. TCR-like stimulation lead to significantly increased variations for such groups of genes, in both directions. **(E)** Overall results pooling three independent screenings, either with (left) 41BB CAR-T cells or (right) CD28 CAR-T cells. log2 fold change for each gene is calculated as average of these values from each individual screening. Sum of rank value is determined as sum of the rankings assigned by MAGeCK alpha-RRA algorithm for each gene in the three screenings. gene-ko subpopulation frequency variations are compared at the endpoint of the experiment, 35 days, vs in starting products.

Figure 8

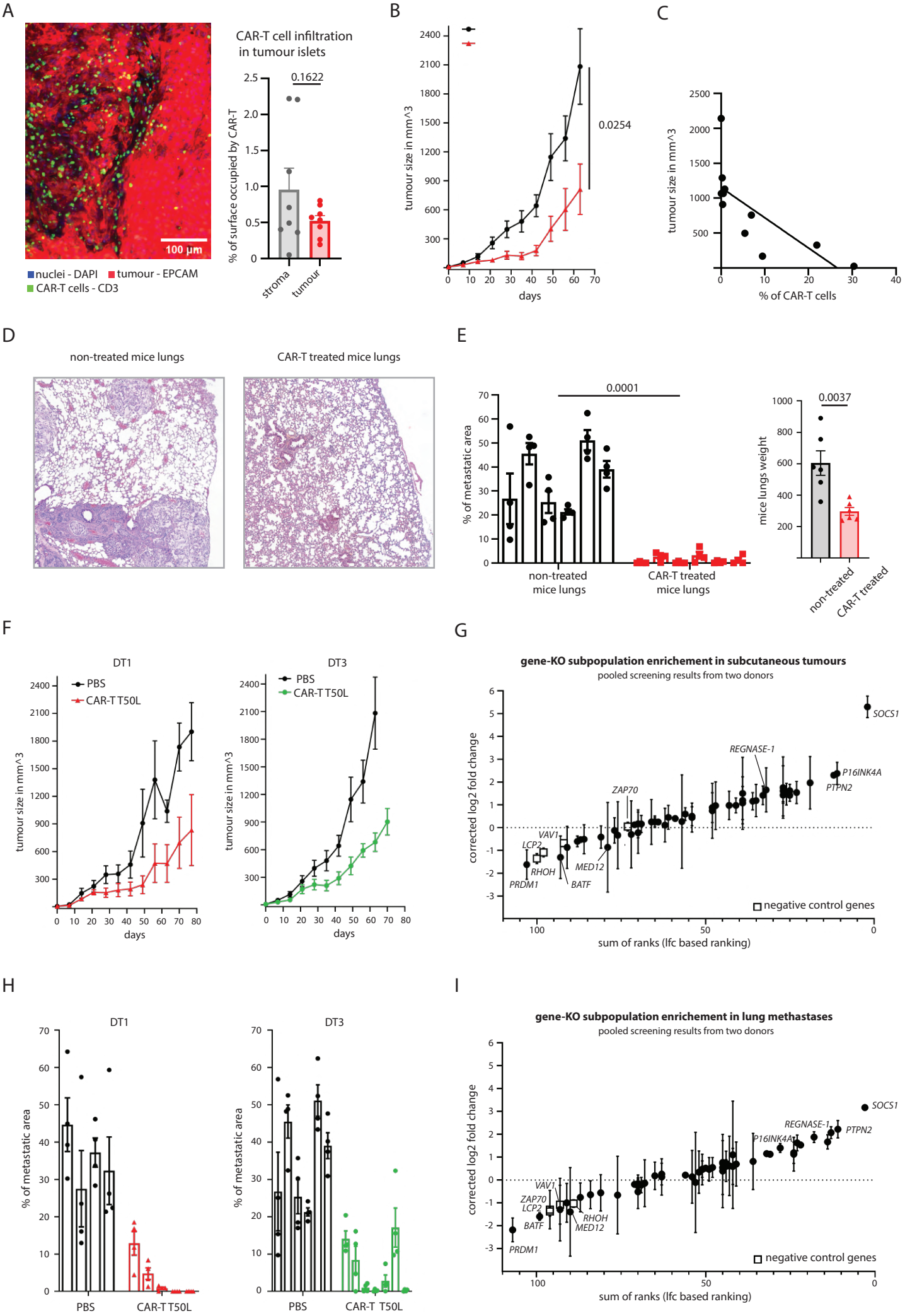
A
100 µm
nuclei - DAPI
tumour - EPCAM
CAR-T cells - CD3
CAR-T cell infiltration in tumour islets
0.1622
% of surface occupied by CAR-T
stroma
tumour
B
tumour size in mm^3
0.0254
days
C
tumour size in mm^3
% of CAR-T cells
D
non-treated mice lungs
CAR-T treated mice lungs
E
0.0001
% of metastatic area
non-treated mice lungs
CAR-T treated mice lungs
0.0037
mice lungs weight
non-treated
CAR-T treated
F
DT1
PBS
CAR-T T50L
tumour size in mm^3
days
DT3
PBS
CAR-T T50L
tumour size in mm^3
days
G
gene-KO subpopulation enrichement in subcutaneous tumours
pooled screening results from two donors
corrected log2 fold change
SOCS1
REGNASE-1
P16INK4A
PTPN2
ZAP70
VAV1
LCP2
RHOH
MED12
PRDM1
BATF
negative control genes
sum of ranks (lfc based ranking)
H
DT1
% of metastatic area
PBS
CAR-T T50L
DT3
% of metastatic area
PBS
CAR-T T50L
I
gene-KO subpopulation enrichement in lung methastases
pooled screening results from two donors
corrected log2 fold change
SOCS1
REGNASE-1
PTPN2
P16INK4A
VAV1
ZAP70
LCP2
RHOH
MED12
BATF
PRDM1
negative control genes
sum of ranks (lfc based ranking)

Figure 8: **(A)** Immunofluorescence microscopy image of A549 cells (Epcam staining in red) subcutaneous tumour, with CAR-T infiltrate (human CD45 staining cells in green). Quantification of CAR-T cells infiltration in tumour mass vs stroma (n=8 tumour slices images) **(B)** Tumour growth curve, assessed by caliper measurements, in mice receiving mock solution (n=5) or treated with 7*10^6 cells(n=5). p-values are calculated by two-ways ANOVA test, results for whole curves comparisons are shown. **(C)** Negative correlation among tumour mass, assessed by caliper measurement, and % of CAR-T cells in mice tumour at the experiment endpoint. **(D)** Haematoxylin-Eosin staining of mice lung slices, showing metastatic burden respectively in treated or not with CAR-T cells. **(E)** Results of machine learning based quantification of metastatic area in subcutaneous tumour bearing mice treated or not with CAR-T cells. (respectively n=20 and 24 images were used for calculation) p-value is calculated by unpaired t-test **(F)** Tumour growth curve, assessed by caliper measurements, in mice receiving mock solution (n=5 for both experiments) or treated with modified CAR-T cells 5*10^6 cells. On the left a first experiment with donor DT1 CAR-T cells (n=5), on the right the same with donor DT3 CAR-T cells (n=6). **(G)** Overall results pooling two independent screenings in the subcutaneous tumour, log2 fold change for each gene is calculated as average of these values from each individual screening. Sum of rank value is determined as sum of LFC based ranking in each experiment, as MAGeCK alpha-RRA ranking loses accuracy in high sample to sample variability conditions. gene-ko subpopulation frequency variations are compared at the endpoint of the experiment, 70 to 77 days, vs in starting products. **(H)** Results of machine learning based quantification of metastatic area in subcutaneous tumour bearing mice treated or not with CAR-T cells. (n=16 and 20 images for CTRL and treated mice were used for calculation for DT1 experiment, n=24 and 24 for the DT3 experiment) **(I)** Overall results pooling two independent screenings in the lungs of mice with subcutaneous tumour, log2 fold change for each gene is calculated as average of these values from each individual screening. Sum of rank value is determined as sum of LFC based ranking in each experiment, as MAGeCK alpha-RRA ranking loses accuracy in high sample to sample variability conditions. gene-ko subpopulation frequency variations are compared at the endpoint of the experiment, 70 to 77 days, vs in starting products.

Figure 9

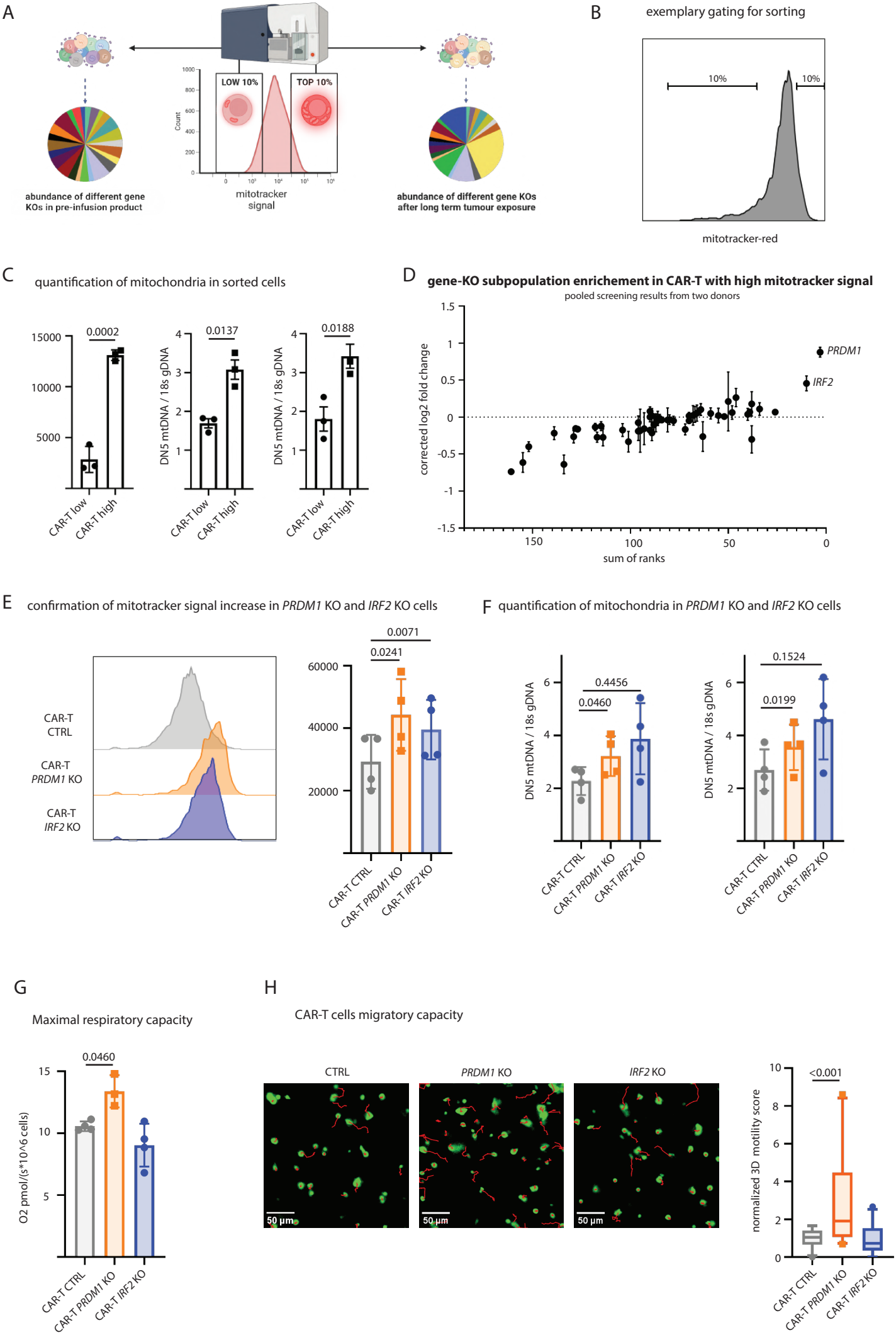
A
LOW 10%
TOP 10%
Count
mitotracker signal
abundance of different gene KOs in pre-infusion product
abundance of different gene KOs after long term tumour exposure
B
exemplary gating for sorting
10%
10%
mitotracker-red
C
quantification of mitochondria in sorted cells
0.0002
0.0137
0.0188
DN5 mtDNA / 18s gDNA
CAR-T low
CAR-T high
D
gene-KO subpopulation enrichement in CAR-T with high mitotracker signal
pooled screening results from two donors
corrected log2 fold change
sum of ranks
PRDM1
IRF2
E
confirmation of mitotracker signal increase in PRDM1 KO and IRF2 KO cells
CAR-T CTRL
CAR-T PRDM1 KO
CAR-T IRF2 KO
0.0071
0.0241
F
quantification of mitochondria in PRDM1 KO and IRF2 KO cells
0.4456
0.0460
0.1524
0.0199
G
Maximal respiratory capacity
0.0460
O2 pmol/(s*10^6 cells)
H
CAR-T cells migratory capacity
CTRL
PRDM1 KO
IRF2 KO
50 µm
<0.001
normalized 3D motility score

Figure 9: **(A)** Schematics of the experiment. **(B)** Exemplary gating for sorting on MitoTracker red signal levels, top 10% and bottom 10% cells have been selected. **(C)** Mitochondrial mass quantification by qPCR measurement of mtDNA copies as compared to genome copies in sorted CAR-T cells. Mitochondrial genes ND1 and ND5 were used for mitochondrial DNA, gene 18s was used for genomic DNA. (n=3 for group) p-values are calculated with one-way Anova test. **(D)** Screening results from three different experiments. gene-ko subpopulation proportions are compared in high vs low MitoTracker signal cells. **(E)** MitoTracker signal levels for CAR-T cells KO for genes *PRDM1* or *IRF2* compared to CTRL ones.(n=4 for group) p-values are calculated with one-way Anova test **(F)** Mitochondrial mass quantification by qPCR measurement of mtDNA copies as compared to genome copies for CAR-T cells KO for genes *PRDM1* or *IRF2* compared to CTRL ones. (n=4 for group) p-values are calculated with one-way Anova test. **(G)** Maximal respiratory capacity as assessed by OROBOROS measurements. (n=3 for *PRDM1* KO, n=4 for CTRL and *IRF2* KO CAR-T) p-values are calculated with one-way Anova test. **(H)** Exemplary migration tracks of CTRL, *PRDM1* KO or *IRF2* KO CAR-T cells in 3D collagen. **(I)** Normalized 3D motility score of CTRL, *PRDM1* KO or *IRF2* KO CAR-T cells. Such score is calculated as product of speed of migrating cell, distance covered and % of actually migrating cells. (n=23 videos) p-values are calculated with one-way Anova test.

Supplementary figure 1

A

CAR-T cell binding to EGFR-protein

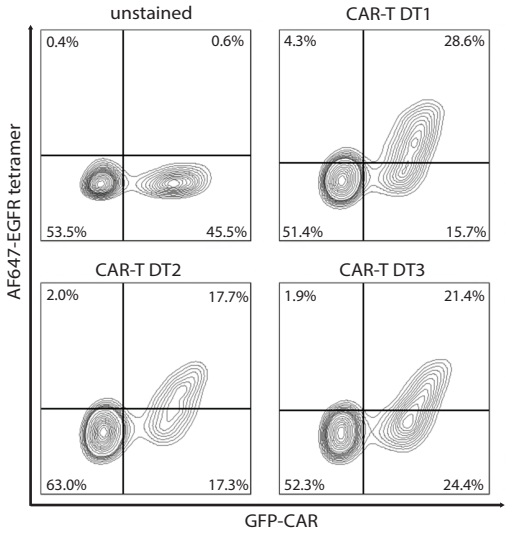

B

CAR-T killing efficacy and specificity

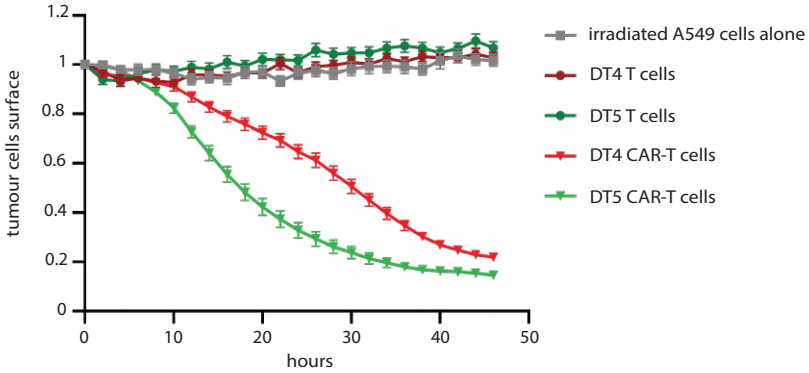

C

CAR-T cells infiltration calculation strategy

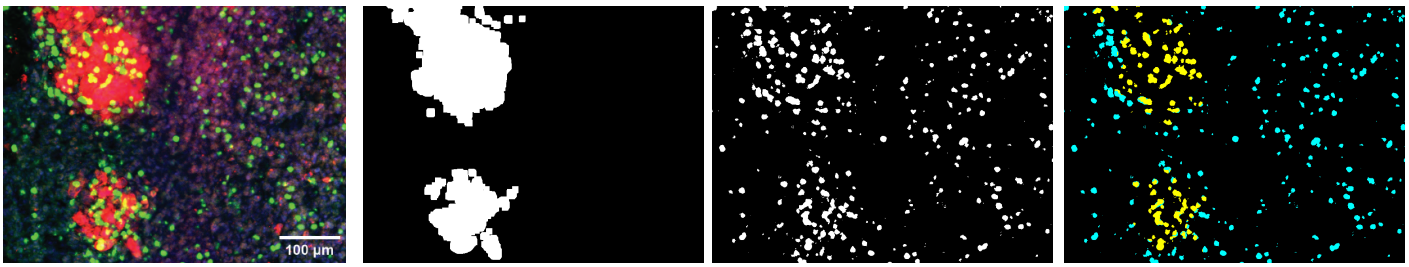

D

CD8 and CD4 CAR-T cell differentiation/exhaustion upon *in vivo* exposure to tumour

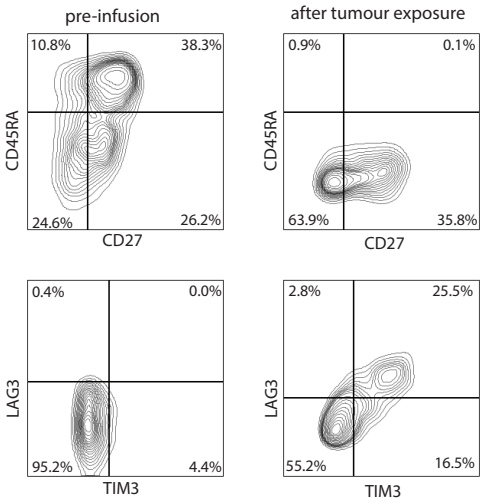

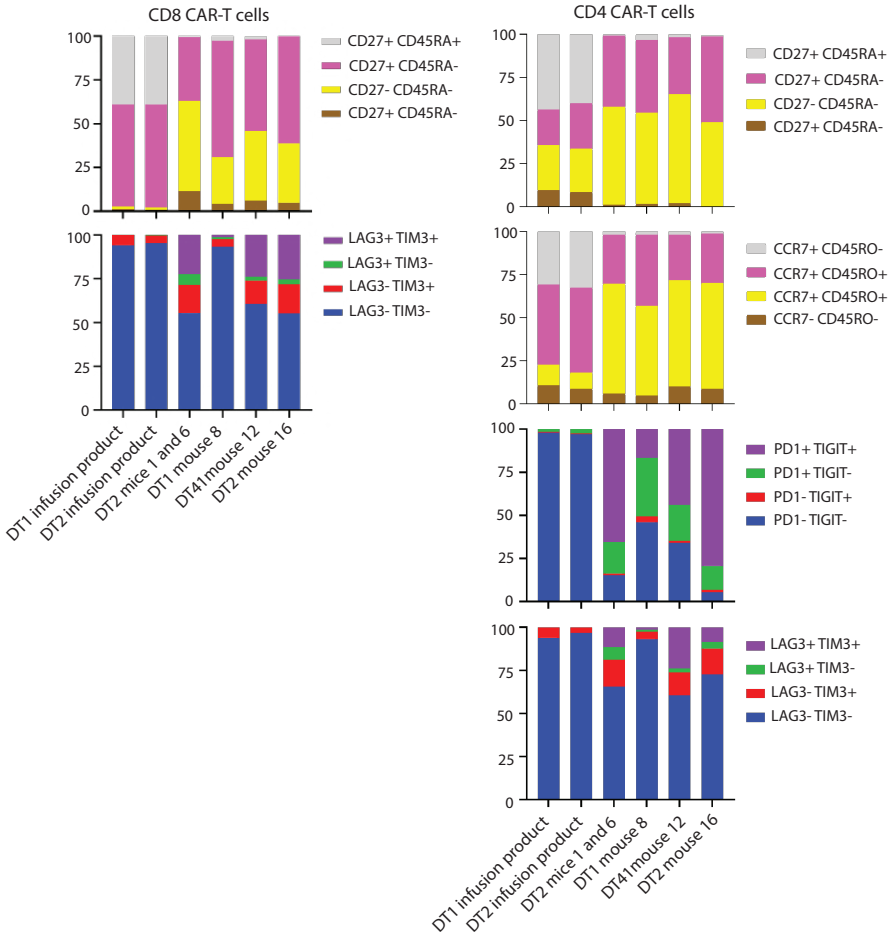

Supplementary Figure 1: **(A)** CAR-T cells binding with biotin-EGFR recombinant protein conjugated in tetramers with A647-streptdadivin. **(B)** CAR-T cells mediated killing of A549 cells as assessed as reduction of mCherry+ area, measured by incucyte imaging. **(D)** CAR-T cells infiltration in tumour islets quantification strategy, from left to right images of different masks used, and merged image of CAR-T cells colocalizing (yellow) or not (cyan) with the EpCAM mask. **(E)** Phenotypical characterisation of CAR-T cells by flow cytometry. We compared CAR-T cells from infusion products and CAR-T cells recovered from mice which received the 5*10^6 dose after long term exposure to tumour *in vivo*.

Supplementary figure 2

A

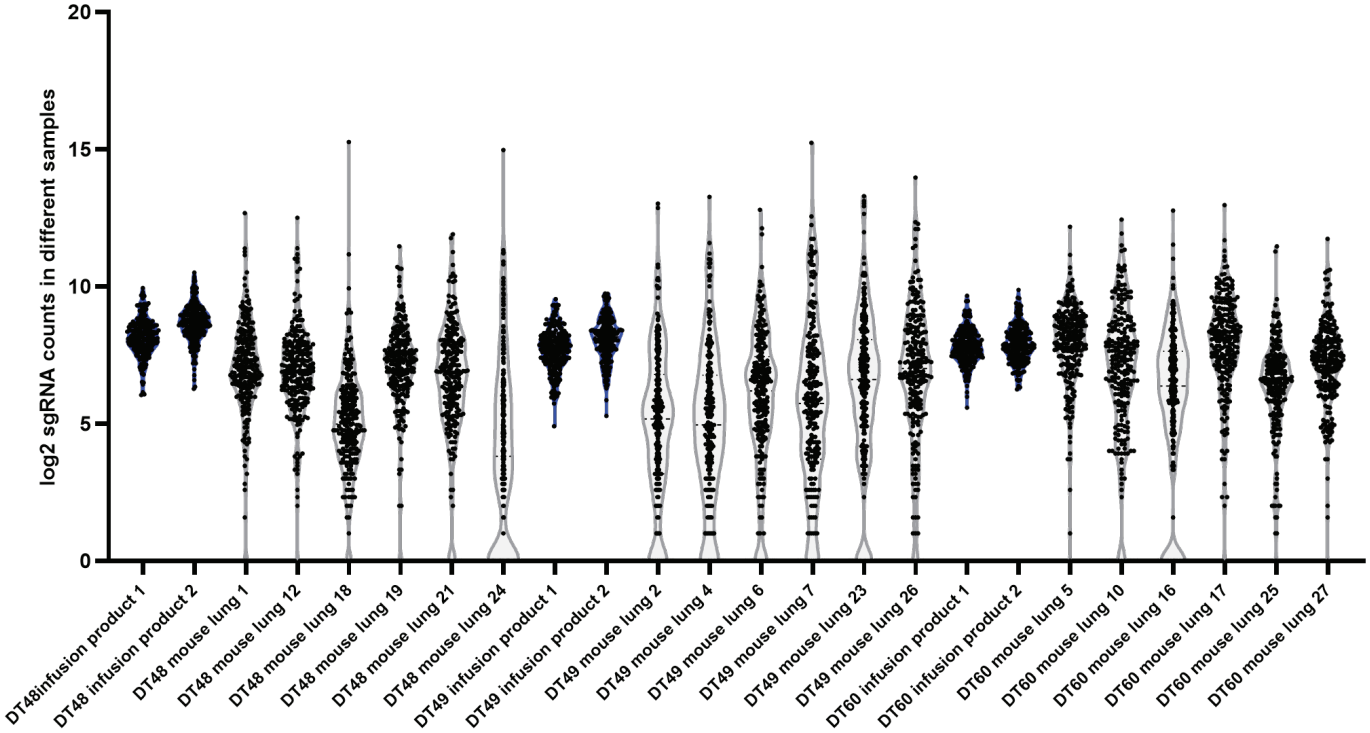

B

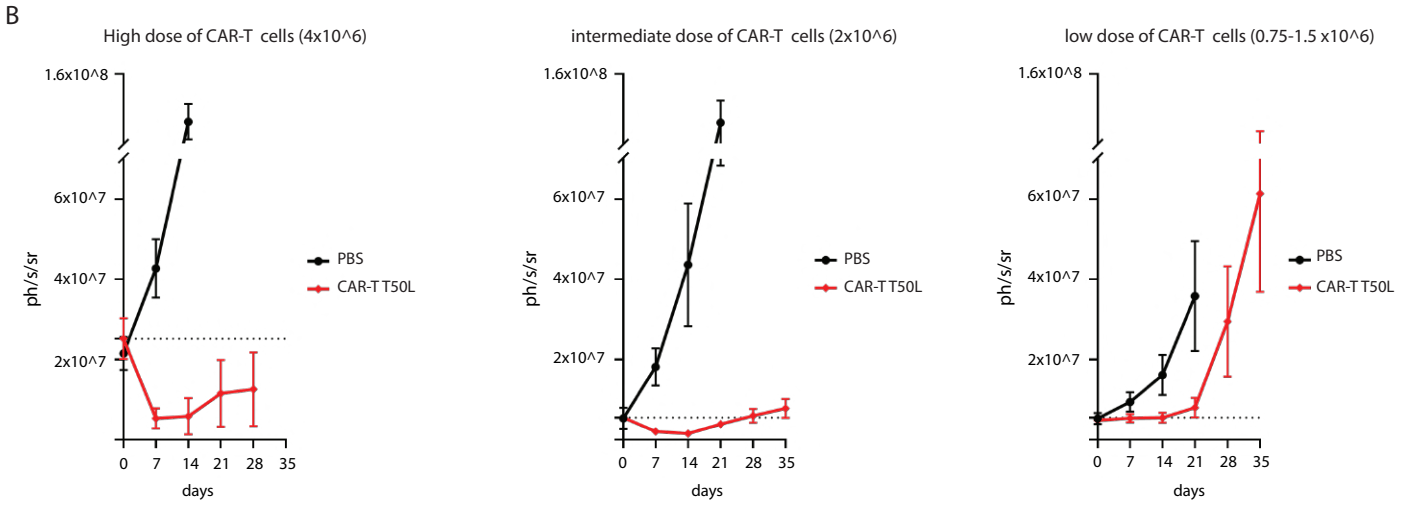

Supplementary figure 2: (**A**) Screening results for CAR-T cells from the three different donors, counts for each sgRNA in log2 axes, counts are compared in mice lungs at the endpoint of the experiment vs in infusion products. (**B**) Tumour growth curves as determined by bioluminescence for mice in different experiments on the same donor CAR-T cells, DT3. Mice first received 10*10^6 A549 cells in the first experiment and 4*10^6 In both the other ones. In the first experiment mice are treated either with excipient (n=5) or 4*10^6 CAR-T modified with our T50L (Top 50 library) lentivirus bank (n=5), in the second experiment they are treated either with excipient (n=5) or 2*10^6 CAR-T modified with our T50L (Top 50 library) lentivirus bank (n=5), in the third experiment they are treated either with excipient (n=5) or 0.75-1.5*10^6 CAR- T modified with our T50L (Top 50 library) lentivirus bank (respectively n=4 and n=4),

Supplementary figure 3

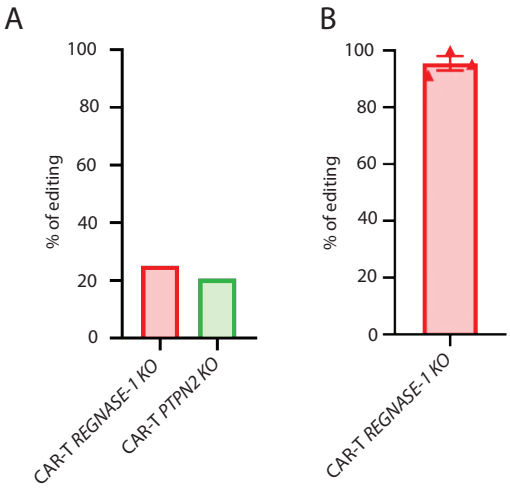

Supplementary figure 3: (**A**) quantification of *REGNASE-1* and *PTPN2* gene editing in CAR-T cells used for the validation in vivo experiments, as evaluated by proportion of modified genomic sequences upon knock out, determined through sanger sequencing and deconvolution analysis of chromatograms files. (**B**) Quantification of *REGNASE-1* gene editing in CAR-T cells used for the in vitro suicide gene experiment, as evaluated by proportion of modified genomic sequences upon knock out, determined through sanger sequencing and deconvolution analysis of chromatograms files. (n=3)

Supplementary figure 4

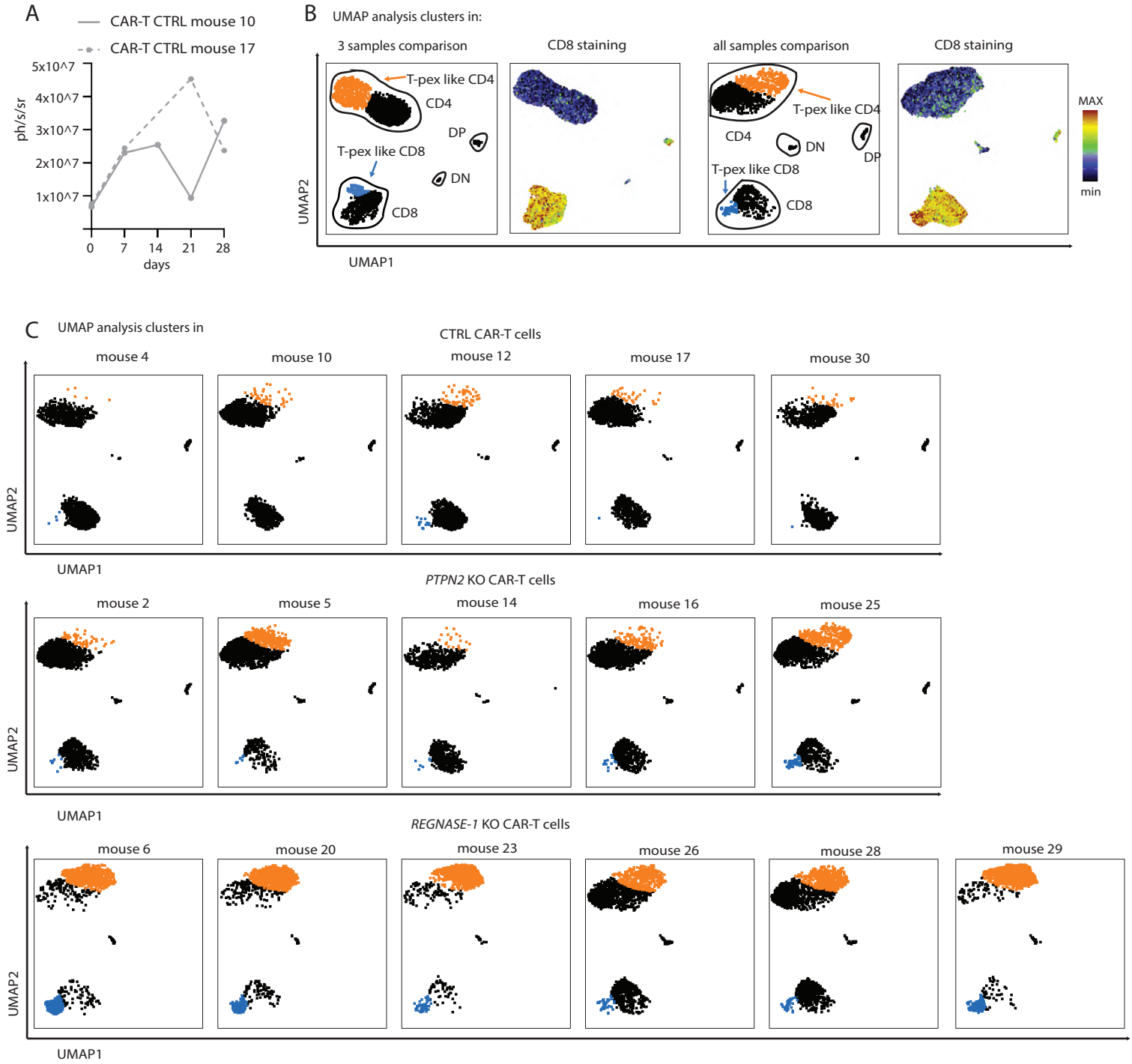

Supplementary Figure 4: (**A**) Tumour growth curve in mice 10 and 17, these mice were excluded from the tumour control comparison experiment, because of excessive tumour burden. These mice were treated with a higher dose of CTRL CAR-T cells, 2*10^6 and were used as additional controls exclusively for the CytOF experiment. (**B**) Comparison of UMAP analysis of CytOF data from CAR-T cells in lung tumour samples at the endpoint of the experiment, either confronting clustering in the analysis with three exemplary samples, as in the main figure 5, or including all samples in the analysis. (**D**) UMAP analysis of CytOF data from CAR-T cells in lung tumour samples at the endpoint of the experiment, in this analysis all samples were included.

Supplementary figure 5

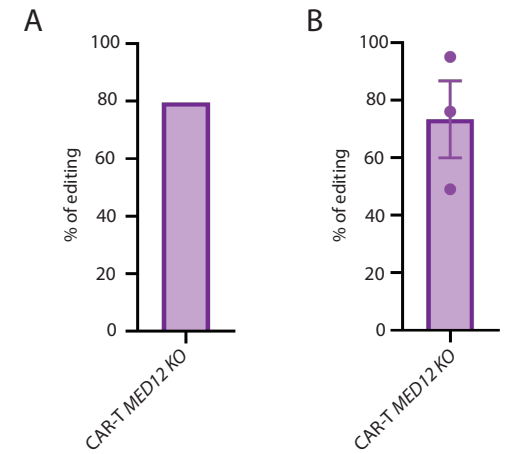

C CD8 and CD4 CAR-T cells differentiation at the end of the production phase

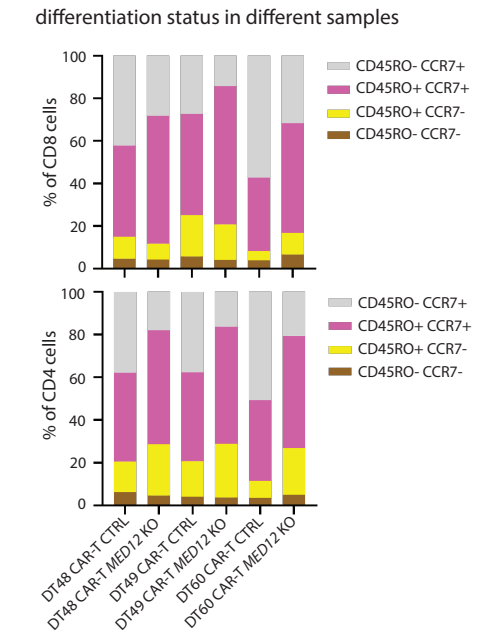

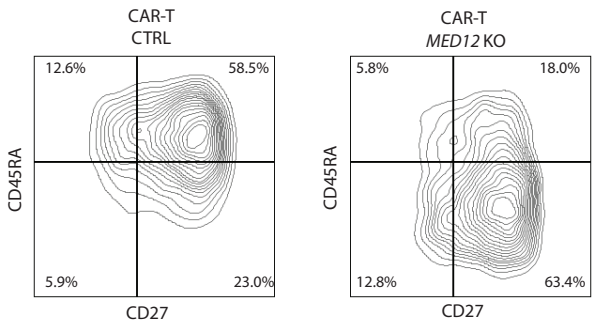

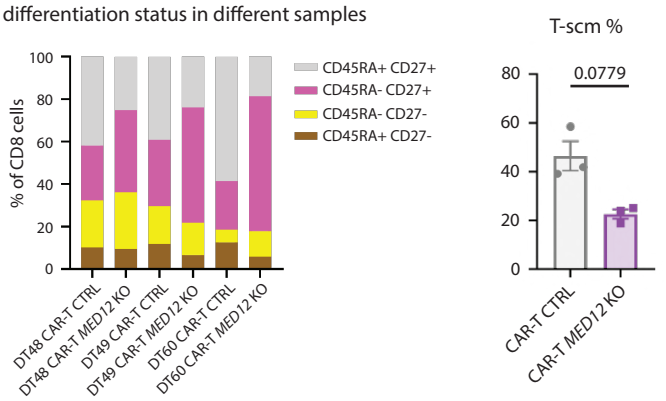

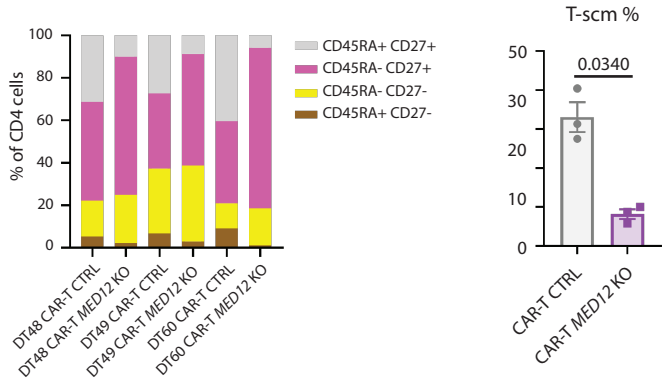

Supplementary figure 5: **(A)** quantification of *MED12* gene editing in CAR-T cells used for the validation in vivo experiment, as evaluated by proportion of modified genomic sequences upon knock out, determined through sanger sequencing and deconvolution analysis of chromatograms files. **(B)** Quantification of *MED12* gene editing in CAR-T cells used for in vitro characterisation experiment, as evaluated by proportion of modified genomic sequences upon knock out, determined through sanger sequencing and deconvolution analysis of chromatograms files. (n=3) **(D)** Flow cytometry-based differentiation profiling for *MED12* KO CAR-T cells as compared to CTRL CAR-T cells at the endpoint of production phase. (n=3 per group) T-scm (T stem cell memory) are here defined as CD45RA+ and CD27+ t-cells, to confirm data from the main figure by a different staining. P-values are calculated with unpaired t-tests.

Supplementary figure 6

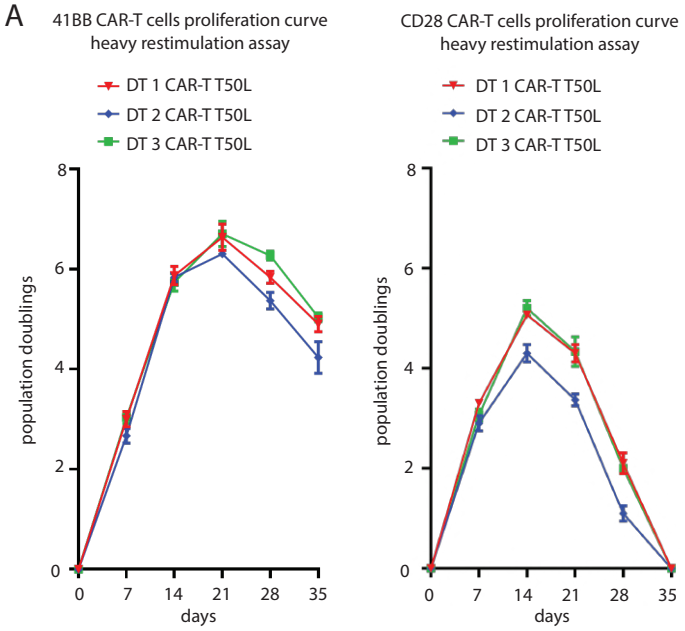

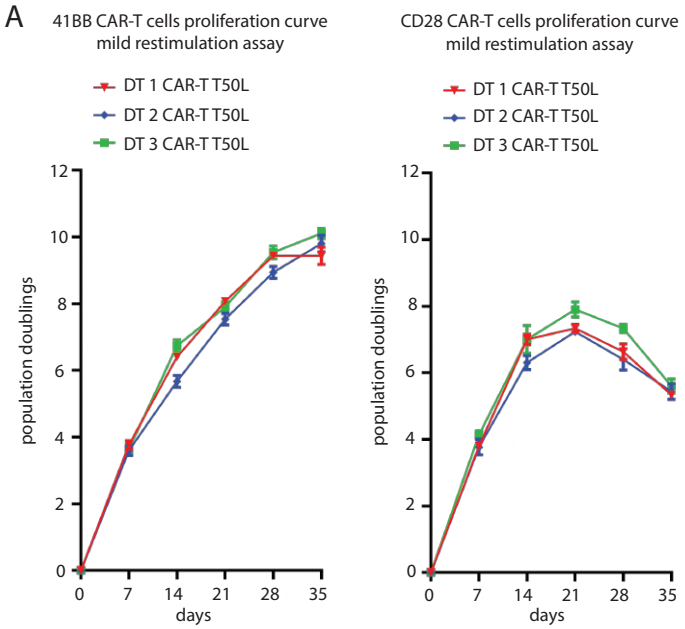

Supplementary figure 6: **(A)** 41BB-CAR-T and CD28-CAR-T cells proliferation curve, expressed in population doublings, in the heavy restimulation assay. Numbers are determined by Trypan Blue corrected cell counting, we cultured 3 replicates for each of 3 donors derived CAR-T cells DT 1, DT 2, DT 3. **(B)** 41BB-CAR-T and CD28-CAR-T cells proliferation curve, expressed in population doublings, in the mild restimulation assay. Numbers are determined by Trypan Blue corrected cell counting, we cultured 3 replicates for each of 3 donors derived CAR-T cells DT 1, DT 2, DT 3.

Supplementary figure 7

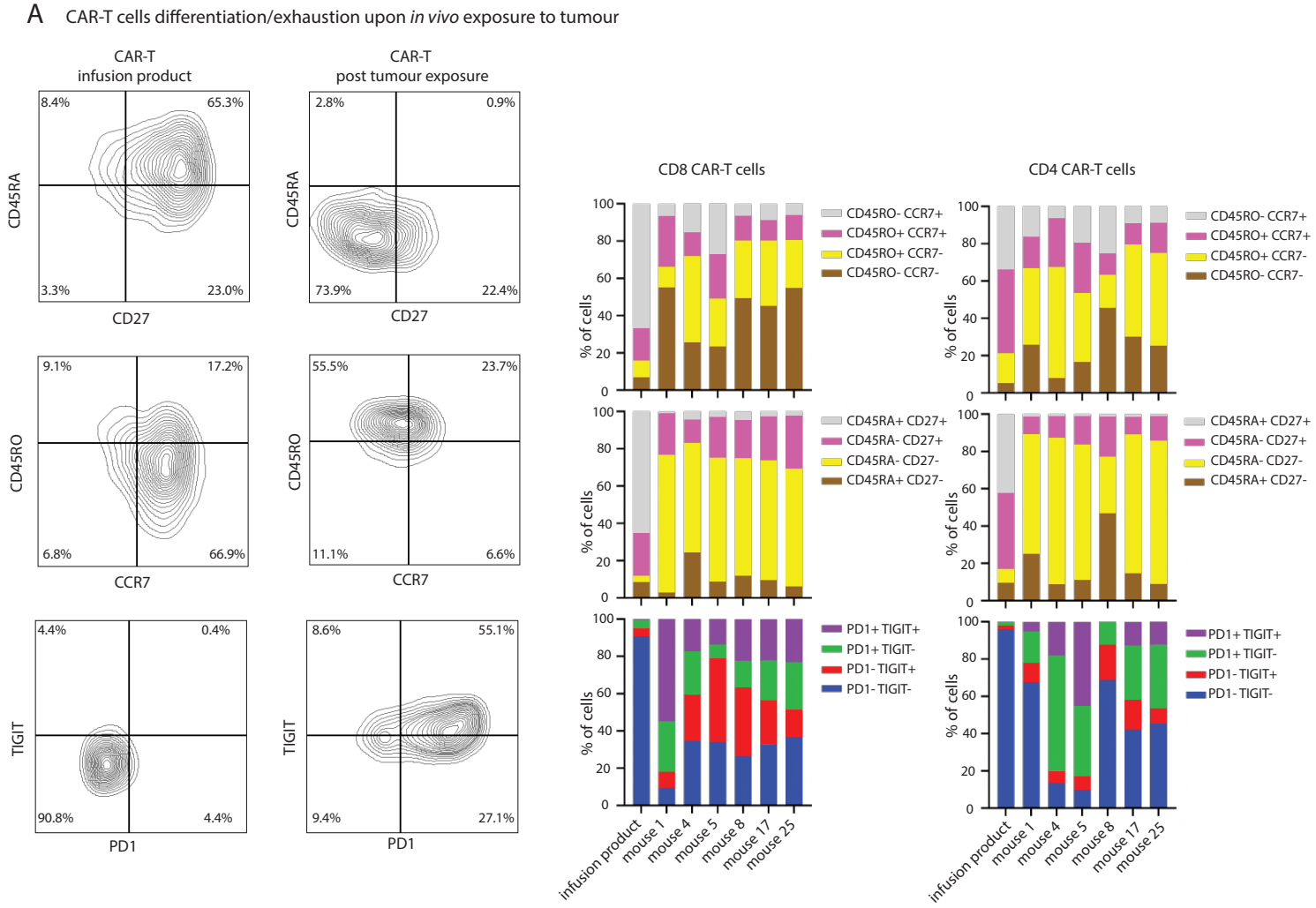

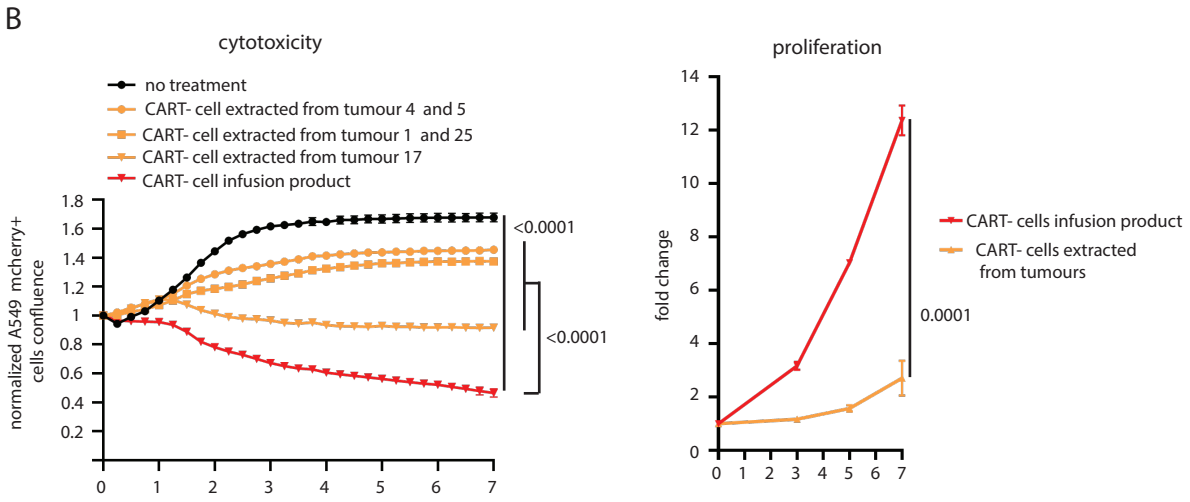

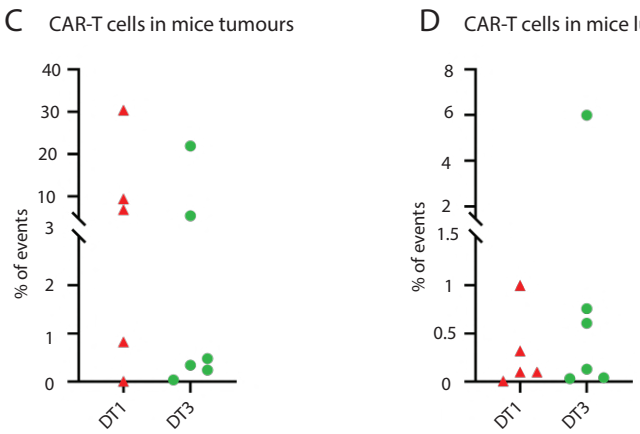

Supplementary figure 7: **(A)** Phenotypical characterisation of CAR-T cells by flow cytometry. We compared CAR-T cells from infusion products and CAR-T cells recovered from mice subcutaneous tumours which received 5*10^6 CAR-T cells, after long term exposure to tumour *in vivo*. **(B)** Functional characterisation of compared CAR-T cells from infusion products and CAR-T cells recovered from mice. Cytotoxic capacity was assessed by calculating surface reduction of mCherry+ tumour cells when co-cultured with CAR-T cells. Proliferation capacity was assessed by cell counting upon 7 days after anti-CD3/C28 stimulation. p-values are calculated by two-ways ANOVA test, results for final time point comparisons are shown. **(C)** CAR-T cells detection in mice subcutaneous tumours and **(D)** lungs by flow cytometry, for DT1 (n=5) and DT3 (n=6)

Supplementary figure 8

A

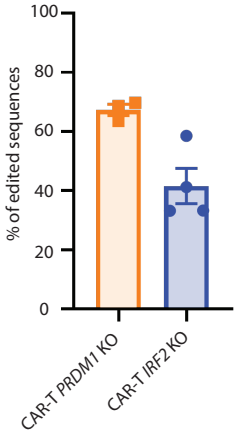

Supplementary figure 8: **(A)** Quantification of *PRDM1* and *IRF2* gene editing in CAR-T cells used for all the in vitro experiments, as evaluated by proportion of modified genomic sequences upon knock out, determined through sanger sequencing and deconvolution analysis of chromatograms files. (n=4 for group)